2008

Development of Effective Balancing Procedure for CT Scanner

Jeremy David Pettinato
Cleveland State University

DEVELOPMENT OF EFFECTIVE BALANCING PROCEDURE FOR CT SCANNER

JEREMY DAVID PETTINATO

Bachelor of Science in Mechanical Engineering

Cleveland State University

May, 2004

Submitted in partial fulfillment of requirements for the degree

MASTER OF SCIENCE IN MECHANICAL ENGINEERING

at the

CLEVELAND STATE UNIVERSITY

August, 2008

This thesis has been approved

for the Department of Mechanical Engineering

and the College of Graduate Studies by

Thesis Committee Chairperson, Dr. Jerzy T. Sawicki

Department/Date

Dr. Ana V. Stankovic

Department/Date

Dr. Hanz Richter

Department/Date

ACKNOWLEDGEMENTS

I would like to thank my advisor, Dr. Jerzy T. Sawicki, for his endless support and guidance he has given me. His involvement has been extremely helpful in the completion of the research work.

Special thanks to Dmitry Storozhev for is countless hours of help in the set-up of the RK-4 test rig. His enthusiasm and support assisted in finishing the laboratory experiment in a timely manner.

I would also like to thank my family and friends for standing by me through my entire graduate studies and my thesis writing. This especially is important that my deepest gratitude goes out to my loving fiancée for her constant understanding and support.

Lastly, I would like to thank Philips Healthcare CT Mechanical for providing me with the material and the support throughout this entire project.

DEVELOPMENT OF EFFECTIVE BALANCING PROCEDURE FOR CT SCANNER

JEREMY DAVID PETTINATO

ABSTRACT

Since the beginning of medical organizations, engineering departments have introduced new innovative ideas and designs to advance image quality. In the case of a CT scanner, one of the largest and most cost effective ways to achieve superior image quality is through a well balanced rotating array. The focus of this thesis is the development of a balancing procedure which will effectively balance a CT scanner rotating array.

Rigid rotor (dynamic) balancing techniques are utilized in order to balance the Philips CT scanner rotor. Upon completion of the dynamic balancing of the CT scanner rotor a new an innovative way to balancing CT scanners is developed. This effective balancing procedure for the CT scanner rotor is proven to be efficient and cost effective when balancing in a high volume manufacturing environment.

TABLE OF CONTENTS

LIST OF TABLES

LIST OF FIGURES

CHAPTER I

INTRODUCTION

The current design for all Computed Tomography (CT) scanners requires a well balanced rotor to generate a fine image quality. The aim for this thesis will be the development of a balancing procedure which will effectively balance a CT scanner rotor. Different balancing strategies for rigid and flexible rotors will be discussed. The flexible rotor balancing technique of influence coefficient method will be used to balance an experimental rotor test rig. The balancing knowledge grasped from rotor test rig will be used to develop a new approach to balancing a CT scanner rotor.

Balancing a rotating machine properly and efficiently is a fundamental step to manufacturing a reliable system. Throughout history balancing procedures and fundamentals have become quite tedious and stagnant. Manufacturing companies back away from the fundamental/routine balancing procedures because they are exceedingly prolonged and costly. This is applicable to the manufacturer as well as the end user of the product. As a result of the costly nature and the extended balancing history many companies are trying to improve their manufacturing process. Corporations are providing faster and less costly ways of balancing their equipment.

Based on the demand for a faster inexpensive balancing procedure, manufacturers of CT scanners are determined to create the most cost effective way to balancing their rotors. The objective of this thesis is to develop a balancing procedure with enough accuracy that the reconstructed images will have no artifacts. Accuracy will ultimately deliver a custom image with high definition. Image quality in the CT world is the most important aspect of the device. There is a constant need to transmit a high quality three dimensional image and reconstruct the image as a precise two dimensional cross section.

The major contributors for poor image quality are artifacts in the reconstructed cross section and image noise. These two facets of poor image quality have many contributors. The main reason behind these defects is the movement of iso-center in the X-ray path from the tube to the detectors. Iso-center is able to move in a three dimensional coordinate system (X, Y, Z). Iso-center is considered to be (0, 0, 0) in Cartesian coordinates and is the theoretical center of the rotating array as seen in figure 1.

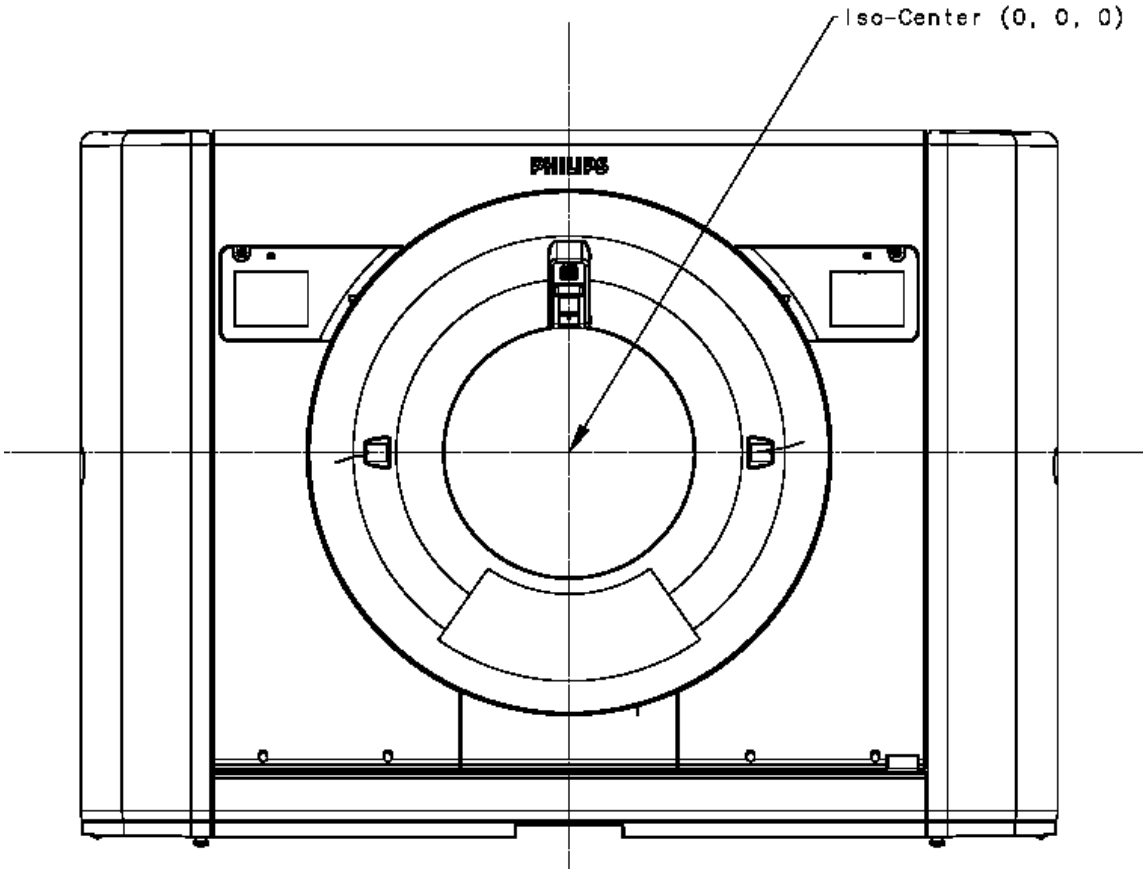

Figure 1: Iso-center Location

Electrical manipulation can be done to minimize the motion at iso-center. Manipulating the focal spot does not always allow itself to be beneficial with image quality. Image quality can easily be overlooked because manipulating the focal spot does not take into consideration movement due to imbalance.

The only way to prevent iso-center motion completely is by balancing the rotating array precisely. The more accurate the balancing is on the rotor the sharper the image quality will be on the reconstructed image. Imbalance of the system is directly proportional to image quality. The more the rotating array moves because of imbalance the harder it is to get a stable iso-center. Although it is almost impossible to completely stabilize iso-center when the CT scanner is rotating at working speeds. Creating precise

balance contributes to a higher stabilization of iso-center than any other method or approach. This is why balancing the rotating array is so crucial in all manufacturing settings of the CT scanner. Not only does it help with certain standard quality practices, but it also prolongs the life of the CT scanner by significantly reducing moments and forces that act on the rotating array.

Basically, this is the fundamental approach to this thesis, i.e., the development of an effective way to balancing a CT scanner. The developed approach must prolong the life of the scanner while also possessing an effective and fast approach. Based on the theoretical approach laid before us for decades a new way of balancing a CT scanner will be developed and proved to provide accurate, effective, and precise image quality for CT manufacturers.

The major contribution to the balancing field would pertain to the way that balancing is performed on a system. This procedure will balance a CT scanner without the help of traditional items (e.g. accelerometers and eddy current probes) but by using a linear transducer to measure the motion. Components inherent to every system will be used to produce phase measurements obsoleting the use of a keyphasor probe. The data from the linear transducer and the CT scanner phase measuring device will be extrapolated and post processed using Matlab. The post processed data will be used to accurately balance the CT scanner rotor.

Chapter 2 of this thesis will start by clarifying the fundamental groundwork and history behind rotor balancing. Various authors and technical publications will be cited. The review of the publications will be provided and discussed so that it can properly

reflect the building blocks and fundamental tools used to develop a new method for balancing a CT scanner.

Chapter 3 will continue on the building blocks set forth from the prior chapter. This chapter will describe the two fundamental types of rotor unbalance. These types of unbalance will be discussed and the different theoretical methods which are used today to balance a rotating array will be presented.

Chapter 4 presents the balancing procedure of flexible rotors using the test rig RK-4 and the Automated Diagnostics for Rotating Equipment (ADRE) system. For demonstration, the influence coefficient method has been selected for rotor balancing. This chapter includes the description of the facility, the procedure, and the obtained results.

Chapter 5 consists of the implementation of the new balancing method on a test CT scanner. The new method for balancing a CT scanner will be formulated and implemented. The implementation will lay the ground work for the procedure for effectively balancing a CT scanner in a manufacturing environment. After this presentation one shall comprehend the conceptual design of the CT scanner. The procedure established for balancing a CT scanner will then be discussed. Upon conclusion of this chapter the evidence of the effectiveness of the balancing procedure for a CT scanner will be recognized. All pertinent data and final results are shown and delivered.

Chapter 6 is the section of conclusions where the results of the testing are discussed. This section will also allow for the discussion of all future work that may come from this research.

CHAPTER II

BACKGROUND

Rotordynamics entirely incorporates theory and practice into its methodology. Rotordynamics was created upon a lineage of innovating trials, although one could easily argue that rotordynamics evolved further through its practice than its theory. This is evident throughout history.

Rotordynamics being a specialized branch of applied mechanics is concerned primarily with the actions and responses to rotating structures. Rotordynamics is concerned primarily with a rotating object which is supported by bearings and rotates about a designated axis. This rotating structure will pass through critical speeds as the speed of the rotating device increases. These critical speeds that the rotor passes through if not balanced can cause catastrophic failure.

Researchers around the world have concentrated on trying to develop balancing practices for the following purposes:

- Increase the overall quality of a device
- Minimize vibration
- Minimize audible and signal noises
- Minimize structural stresses

- Minimize fatigue
- Increase the overall life of the bearing
- Minimize power loss

These aspects are the fundamental driving conditions as to why rotordynamics is constantly evolving throughout history.

In 1869 Rankine was the first to perform an analysis of a spinning shaft. Rankine suggested that the super critical speeds of the shaft could not be attained (Foiles, 1998). Rankine's analysis was then subsided years later when Dunkerley published a paper (Foiles, 1998) explaining how the shaft reaches supercritical speeds. Dunkerley's practice then led to others obtaining super critical speeds through the shaft, including Carl Gustaf De Laval, in 1889, (Foiles, 1998) ran a steam engine to super critical speeds while in 1895 A. Foppl formulated and solved the equations governing the response of a single mass un-damped rotor system (Foppl, 1895).

Throughout the years H.H. Jeffcott, in 1919, explained the fundamental response of a single mass flexible rotor to unbalance (Jeffcott, 1919). Based on Jeffcott's studies the theory of shaft whirl was eventually established and because of this research Jeffcott can be considered the starting point for later research. This was the first major step in the rotor balancing techniques. Though Jeffcott could explain whirling due to unbalance in his terms; his analysis left various instability phenomena unexplained (Bishop, 1959). Even though Jeffcott's approach gave a simple mathematical picture of whirling occurrence the theory is not suitable for the quantitative analysis of real rotors, for which it was never intended (Bishop, 1967).

The next major step in the field of rotordynamics came from E.L. Thearle in 1934 (Thearle, 1934). Thearle's method was developed for one and two plane balancing of rotors at a given speed by placing trial weights at either end of the machine and measuring the response at each end due to the individual weights. This procedure is still being used today with great success and is in essence the fundamental groundwork in which the influence coefficient method was derived for multi-mass rotors (Foiles, 1998).

J.G. Baker furthered Thearle's work in 1939 in his paper (Baker, 1939). Baker's work suggests using groups of trial weights which affect the vibration at only one bearing at a time at a given speed (Baker, 1939). He explored this on machinery with two and three bearings; with such a technique one could balance multiple planes with essentially a single plane balance computation.

It wasn't until 1959 that R.E.D Bishop wrote a document on The Vibration of Rotating Shafts (Bishop, 1959). In this particular paper Bishop's purpose was to relax the usual assumptions in the analysis of rotating shafts. He formulated a more complete theory to balancing flexible shafts and made new advances in the tribulations of stability. Bishop allowed a way to incorporate bearing characteristics while also suggesting methods for lack of axial symmetry.

Again in 1959 Bishop and Gladwell introduced what is thought of as the modern day modal balancing technique. This paper (Bishop and Gladwell, 1959) delineates the motion of flexible unbalanced rotating shaft. They explain the effects of balancing such a shaft (as a rigid body) in a conventional low-speed balancing machine. The overview of the document is based upon balancing flexible rotors mode by mode. The paper also shows how dead weight of the rotor effects the deflection of the rotating shaft.

All of these researchers provided ground breaking technological advances in the balancing fields and all of these methods are still used today to some extent in rotordynamics. They have provided the foundation for the modern day world and since their inception they have been expanded upon numerous times. The unified approach for example was developed in order to take the advantages of both modal and influence coefficient and use them as one holistic balancing approach.

Gunter, Barrett and Allaire, in 1976, concluded that the combination of modal balancing and influence coefficient method may result in the optimum technique for flexible multi-mass rotors (Gunter et al., 1976). This technique was also reassured by Darlow. Mark S. Darlow, in 1987, published a paper on balancing of high-speed machinery (Darlow, 1987). This paper strived to describe the three principle flexible rotor balancing methods: modal balancing, influence coefficient balancing, and the unified balancing approach. Darlow demonstrates that based on the results of his paper that the superior balancing technique is the unified balancing approach. Darlow provided the important information of the ill-conditioning of the balancing equations.

Based on the original balancing techniques: influence coefficient, modal, and unified approach there have not been any other major contributions as a standalone balancing technique. Most of the modern day researchers all use these three balancing techniques with slight modifications and simplifications in order to provide a more cost effective and quicker way of balancing rotating machinery. These aspects can clearly be seen in Tan and Wang's research (Tan and Wang, 1993). They developed an introduction to low speed balancing of flexible rotors through the unification and further development of the modal balancing and influenced coefficient techniques. Their research consisted of

taking two of the main techniques in modern balancing, modal and influence coefficient, and establishing a unified expression for both techniques. Their theory of unified approach incorporates the procedure and defense that flexible rotors can be balanced at low speeds, so that high speed balancing is not needed once certain criteria is met.

This low speed balancing technique was again displayed in Shi's document (Shi, 2005) on a modified low-speed balancing method for flexible rotors based on the holospectrum technique. In 2005, Shi researched the low speed balancing technique that Tan and Wang described in their document (Tan and Wang, 1993). Shi further developed a procedure for balancing rotors at low speeds instead of high speeds as well. Techniques that were previously used caused significant losses in capital, time, and exhausted man power. Shi also explained how complicated and dangerous it was when using such high speeds to balance the rotating machinery.

Instead Shi delivers an approach of Low Speed Holo-Balancing (LSHB) (Shi, 2005), which balances flexible rotors without test runs at high speeds. LSHB is primarily based on the holospectrum technique. Instead of using a single sensor one is able to use multi-sensor fusion to describe a three-dimensional holo-spectrum with the following specialties. The first specialty enables one to analyze the vibrational response of a rotor described by a three-dimensional holospectrum with multi-sensor fusion, instead of information from a single sensor. Secondly, the variation rules are studied in the run-up and run-down stages. This enables LSHB to proficiently balance flexible rotors at lower speeds other than the first critical speed, according to the decomposition results of the holo-spectrum. Finally, this process allows for the first two modal components to be corrected simultaneously at a speed below the first critical speed. LSHB is set apart from

traditional balancing practices because it does not need any test runs at any speeds higher than the first critical speed. LSHB brings to the balancing field a much more versatile way of balancing a rotor solely based on the safety and cost efficiency.

Furthermore, in the extensive research of balancing procedures the next researcher G.A. Hassan developed (Hassan, 1995) a new approach for computer-aided static and dynamic balancing of rigid rotors. Hassan developed a new "black box" approach to balancing. The black box approach minimizes the amount of trials. It uses regression analysis to relate particular vibrational amplitudes at one or two different rotor bearings to the balancing variables (weight, mass, and phase angle). A powerful optimization program is used to minimize an objective function combining the vibrational levels at both supports (bearings) with pre-assigned weighting constraints being subject to constraints on the balancing variables. The astounding aspect about this procedure is that it can be applied to both static and dynamic balancing of rigid rotors. Overall, Hassan achieved an 83.7% reduction in vibrational levels. This approach, although it is an applied rigid rotor balancing technique, may be of some interest in other dynamic problems (e.g. non-linear support characteristics, fine balancing, variable speed rotors, and flexible rotors).

Hassan evolved the black box approach to incorporate the aspects of down time, training requirements, and minimization of labor cost. The procedure is a cohesive approach that could be used in many balancing situations. This procedure is very cost effective to implement in any manufacturing environment.

Lastly, Xu and Qu developed a new practical method for rotor balancing in 2001 (Xu and Qu, 2001). This new practical method for modal balancing uses the modal ratio

among measurement points (MRMP coefficient). The new method is an improvement on traditional modal balancing because the rotor operates at speeds between the first and second critical speeds. MRMP coefficient is introduced for the first time in this paper (Xu and Qu, 2001), strictly on the basis of the rotor-bearing system being balanced at any particular rotor speed between the first and second critical speeds. This is preformed primarily by decomposing the modal components of unbalance and response simultaneously.

Based on these documents stated throughout this section many new approaches and theoretical values have been described. Many of the procedures and practices defined are very unique in their own nature and content. All the documents provide ground breaking techniques that will ease the balancing procedure and the cost of performing rotor balancing.

These procedures above all have an inherent value. They all need expensive equipment such as accelerometers, probes, control boards, or other balancing components that are not listed in the researchers' procedures. These are the hidden costs in all balancing practices. They are not discussed in a relative sense in any of the author's articles. The time reduction and cost savings is on the piece parts level (single units). Based upon a manufacturing outlook there is an exuberant amount of cost that goes into producing mass quantity systems. The need for a balancing system that minimizes training, downtime, and the cost for the overall product being shipped is critical for corporate America.

CHAPTER III

THEORY

There are several different types of balancing practices. All of these practices share the same fundamental terms that are used throughout the balancing procedure. The fundamental terms that are intrinsic to all balancing practices are listed below:

- Mass Center
- Center of Gravity
- Axis of Rotation
- Principal Inertia Axis
- Centrifugal Force
- Moment and Couple

These terms are the back bone to why and how balancing is performed. Balancing is such a broad arena of research that practices have been broken down into two different categories. The first category is rigid rotor balancing while the second practice is flexible rotor balancing. When choosing which imbalance category to employ one must understand the rotordynamic behavior and the different types of unbalance.

A. TYPES OF UNBALANCE

a. STATIC UNBALANCE

This is the relocation of the mass center in one or more directions to a specified point in space by the rearrangement of mass within the system or the addition of mass at appropriate coordinate values. Static unbalance (Force Unbalance) is the easiest type of unbalance to eliminate. Static unbalance also has another condition which involves the rotational axis lying parallel to the central principal axis which means there is no uncouple balance. Static unbalance is usually expressed in terms of weight and length or $U = Wr$. Where W is the weight and r is the effective radius of the weight this can be seen in figure 2 below.

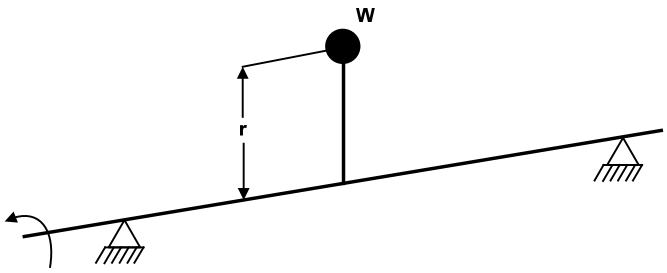

Figure 2: Static Balance Depiction

When a rotor is in static balance the mass center lies on the axis of rotation. This can be seen in figure 3 below. When this condition exists the part can spin on the axis with no inertial forces; without generating centrifugal force. These unbalance forces can be corrected by adding correction masses to the rotating array and shifting the mass center of the rotor onto the axis of rotation.

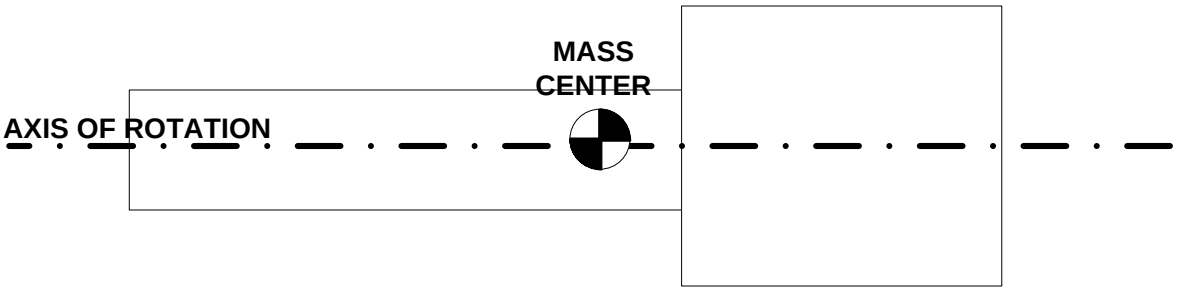

Figure 3: Static Equilibrium

b. COUPLE UNBALANCE

In this particular situation, as seen in figure 4, the central principal axis of inertia is not parallel with the rotational axis and the mass center lies on the axis of rotation so there is no static unbalance.

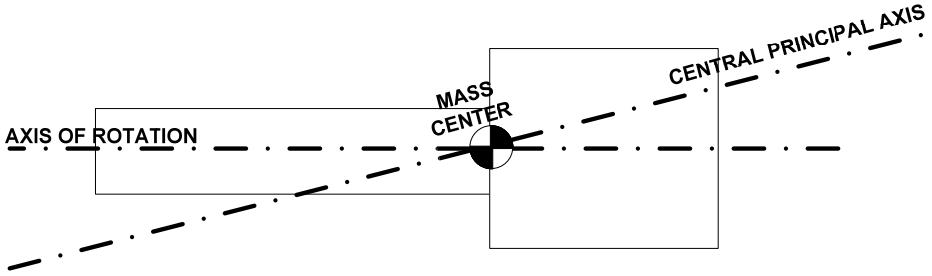

Figure 4: Couple Unbalance Depiction

Couple unbalance is defined in units of weight and length^2 or $U = Wrd$ where W is the weight, r is the effective radius, and d is the couple arm. This can be seen in figure 5 below.

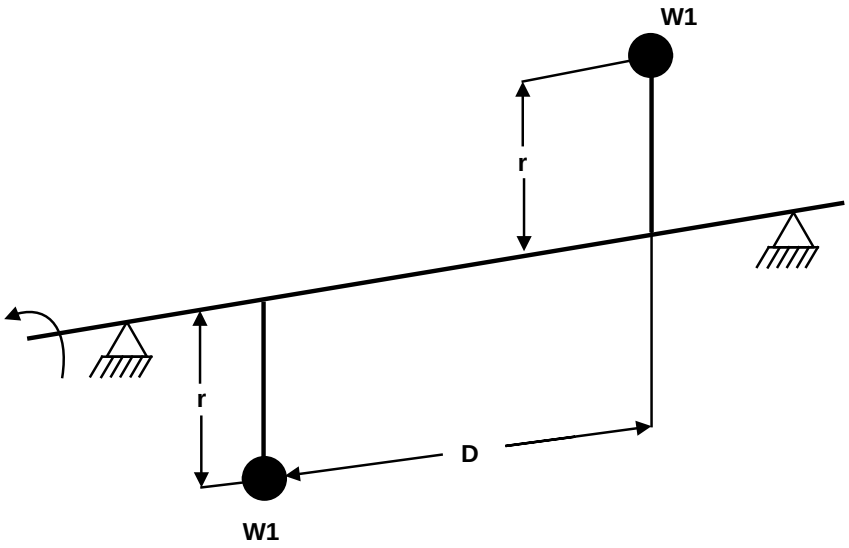

Figure 5: Equation Example

In order to correct couple imbalance on a rotor two equal weights must be placed 180^0 apart in two different correction planes. The distance between these planes is the couple arm. This correction plane is provided arbitrarily and the product of *Wrd* matches the unbalance.

c. DYNAMIC UNBALANCE

The problem of dynamic balancing is somewhat different than static balancing; hence a system which is statically balanced is not necessarily dynamically balanced. In dynamic balancing, the significant parameters are the masses of the members and a distance squared. The squared distance arises from the forcing function and the moment arm dimension. The forcing function for dynamic balancing is usually due to the rotation of the system and is oriented in the radial direction (centrifugal force). The moment arm has the same interpretation as for the static balancing case. Basically, the central principal axis is neither parallel nor intersecting the rotational axis as seen in figure 6.

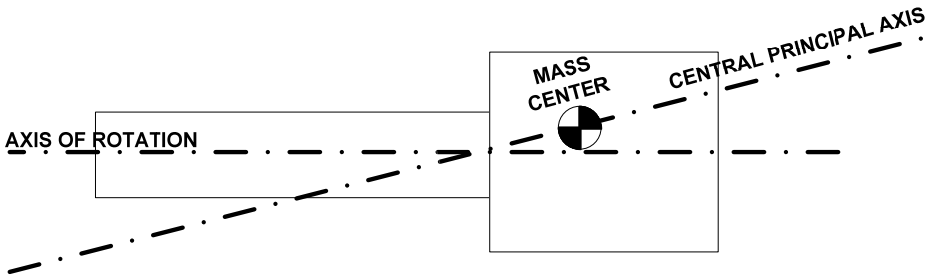

Figure 6: Dynamic Imbalance Example

Dynamic imbalance can also be referred to as two plane unbalance; this is representative of correction masses needed in two planes in order to eliminate unbalance. Two plane balances can be written in terms of *Wr* and must include axial locations of the specified correction planes. This is depicted in figure 7 below.

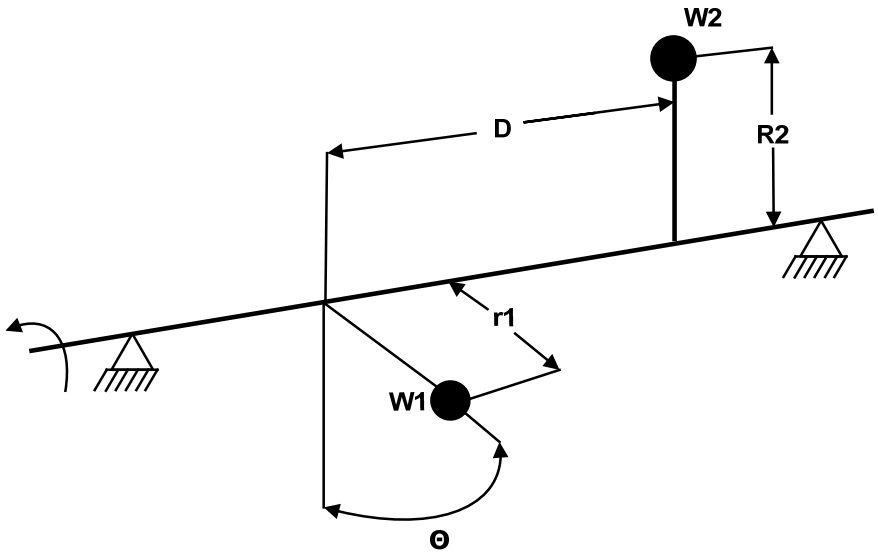

Figure 7: Dynamic Imbalance Example

d. QUASI-STATIC UNBALANCE

Quasi-static unbalance, as seen in figure 8, is the special case of dynamic unbalance in which static and couple unbalance vectors lie in the same plane. When a correction mass is altered on the rotor in a particular plane from the mass center at some distance a static unbalance is created as well as a couple unbalance. Quasi-static

unbalance can be balanced with a single correction mass if it is the right magnitude and in the right plane.

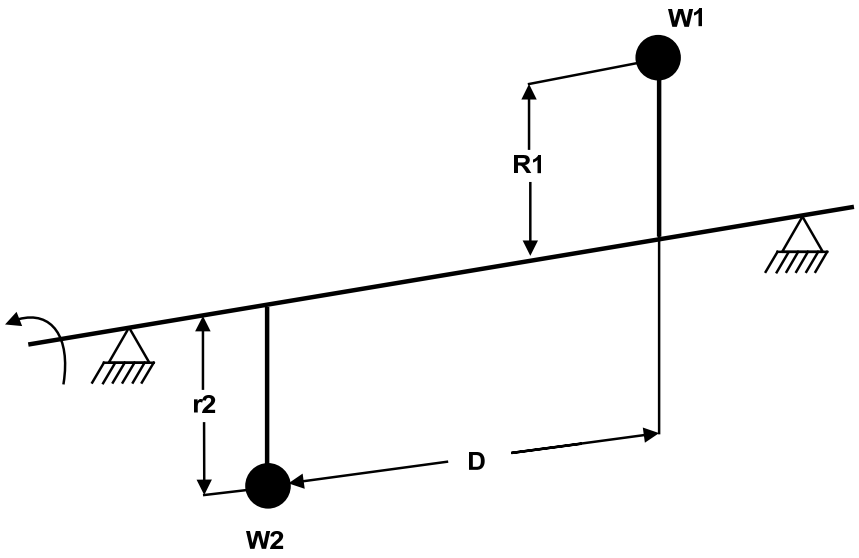

Figure 8: Quasi-Static Unbalance Example

B. RIGID ROTOR BALANCING

Rigid rotor balancing has numerous procedures and tools which are very well established in the balancing field. Most of the techniques are very straight forward in their approach, both mathematically and theoretically. Rigid rotor balance is when the shape of the centroidal axis is not a function of speed. There are two different procedures combined into rigid rotor balancing, i.e., static and dynamic balancing. Using the rigid rotor technique the rotor is balanced to a point where the individual is able to get the desired speed without having complications. Static and dynamic balancing techniques are described below.

a. STATIC BALANCING

Static balancing is the relocation of the mass canter in one or more directions to a specified point in space by the rearrangement of mass within the system or the addition of mass at appropriate coordinate values.

Static balancing eliminates system motion in only one plane (X-Y plane) or the plane synchronous with rotation. The balance is accomplished by locating the center of gravity (CG) of the rotating load at the axis of rotation (0, 0, 0). Therefore, satisfying the equations:

$$S_x = -\sum_i m_i y_i = 0 \quad \text{Static x moment} \tag{3.1}$$

$$S_y = \sum_i m_i x_i = 0 \quad \text{Static y moment} \tag{3.2}$$

where m_i: mass of component i.

x_i, y_i: coordinates of components

If $S_x \neq 0$ or $S_y \neq 0$, the additional mass required at radius R_{cw} is found by:

$$M_{scw} = \frac{\sqrt{S_x^2 + S_y^2}}{R_{cw}} \quad \text{Static balance weight} \tag{3.3}$$

This is located at an angle of:

$$\Theta_{scw} = \tan^{-1}\left(\frac{-S_x}{S_y}\right) \quad \text{Static balance weight location} \tag{3.4}$$

And at and (x, y) coordinate:

$$X_{scw} = R_{cw} \cos\Theta_{scw} \tag{3.5}$$

$$Y_{scw} = R_{cw} \sin\Theta_{scw} \tag{3.6}$$

b. DYNAMIC BALANCING

In dynamic balancing, the significant parameters are the masses of the members and a distance squared. The squared distance arises from the forcing function and the moment arm dimension. The forcing function for dynamic balancing is usually due to the rotation of the system and is oriented in the radial direction (centrifugal force). The moment arm has the same interpretation as for the static balancing case. Figure 9 shows an illustration of how the first moment should be calculated.

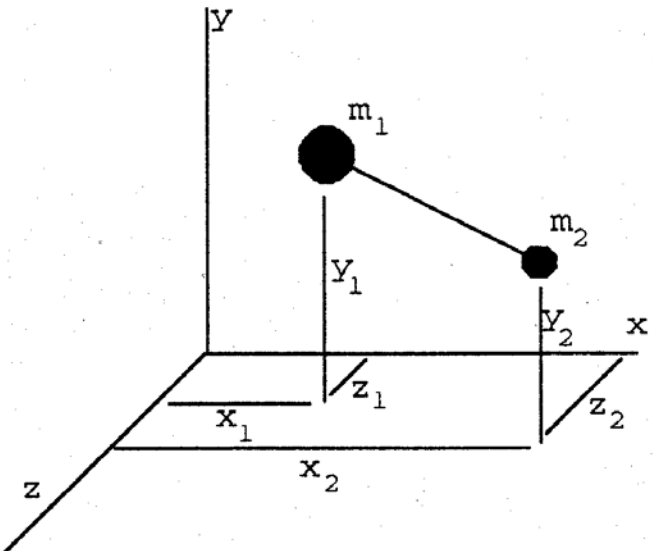

Figure 9: Illustration of First Moment Calculations

$$T = rF \tag{3.7}$$

where T is the torque vector, r is the position vector, and F is the force vector for each point in the system. The position vectors are as follows:

$$r_1 = x_1 i + y_1 j + z_1 k \tag{3.8}$$

$$r_2 = x_2 i + y_2 j + z_2 k \tag{3.9}$$

Assuming that the system exhibits constant rotation about the Z-axis, the forcing function can be expressed as:

$$F_1 = (m_1 a_{1x})i + (m_1 a_{1y})j \tag{3.10}$$

$$F_2 = (m_2 a_{2x})i + (m_2 a_{2y})j \tag{3.11}$$

where a_{1x}, a_{1y}, a_{2x}, and a_{2y} represent the x and y components of the acceleration of masses 1 and 2. Referring to figure 10 below, these forces can be expressed as:

$$a_{1x} = -r_1\omega^2 \cos(\Theta_1) \tag{3.12}$$

$$a_{1y} = -r_1\omega^2 \sin(\Theta_1) \tag{3.13}$$

$$a_{2x} = -r_2\omega^2 \cos(\Theta_2) \tag{3.14}$$

$$a_{2y} = -r_2\omega^2 \sin(\Theta_2) \tag{3.15}$$

where r_1, r_2, Θ_1, and Θ_2 are the hypotenuse and angle with the x and y axes for the two masses respectively. Equations 3.12 through 3.15 can be further simplified by observing that the sine and cosine functions can be expressed in terms of x, y, and r:

$$\sin(\Theta) = y/r \tag{3.16}$$

$$\cos(\Theta) = x/r \tag{3.17}$$

Upon substituting equations 3.12 through 3.15 into equations 3.10 and 3.11, the following expressions for the forcing function results:

$$F_1 = (-m_1 x_1 \omega^2)i - (m_1 y_1 \omega^2)j \tag{3.18}$$

$$F_2 = (-m_2 x_2 \omega^2)i - (m_2 y_2 \omega^2)j \tag{3.19}$$

Substituting the position vectors (equations 3.8 and 3.9) and the forcing function vectors (equations 3.18 and 3.19) into the equation for the torques (equation 3.7) gives:

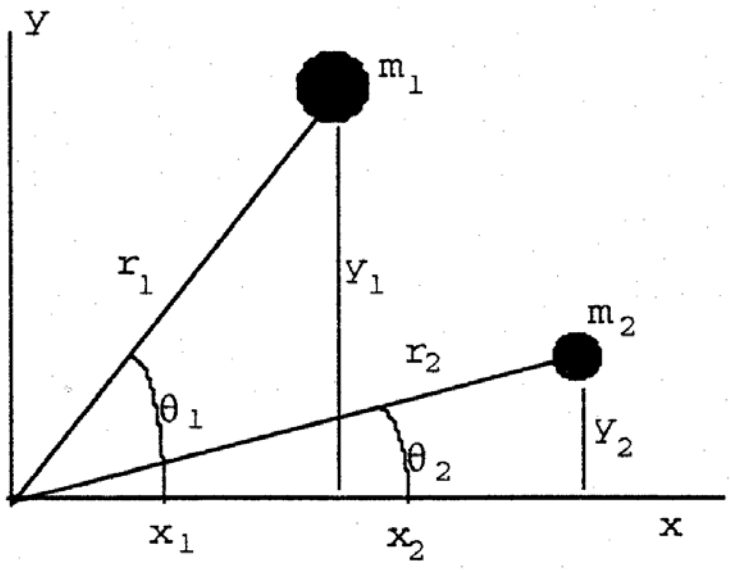

Figure 10: Illustration of Geometry looking down the Z-axis

$$T_1 = \left(m_1\omega^2 y_1 z_1\right)i - \left(m_1\omega^2 x_1 z_1\right)j \tag{3.20}$$

$$T_2 = \left(m_2\omega^2 y_2 z_2\right)i - \left(m_2\omega^2 x_2 z_2\right)j \tag{3.21}$$

Notice that there is no z-direction component. Rotation about the z-axis produces imbalance torques only about the x and y axes. The total torque vector due to all the masses in the system is more useful than the torques of the individual elements so:

$$T = \sum T_i = T_1 + T_2 \tag{3.22}$$

Since the system rotates about the z-axis, the torque vector is not constant in the i and j directions but is a harmonic progression. Consequently, the resultant magnitude of the torque vector is most useful in evaluating the dynamic imbalance:

$$T = \omega^2 \times \sqrt{\left(m_1 y_1 z_1 + m_2 y_2 z_2\right)^2 + \left(m_1 x_1 z_1 + m_2 x_2 z_2\right)^2} \tag{3.23}$$

C. FLEXIBLE ROTOR BALANCING

Based on the fact that vibrational modes involve simultaneous vibrational interactions between all coupled components (e.g. rotor, casing, foundation, attached masses, etc.) can be referred to as system mode shape. The rotor moves (precesses) in an orbit and this precession produces a set of rotational reaction forces in the bearings. These forces are transmitted throughout the entire system and respond dynamically to the rotating forces. Rotor mode shapes are strongly influenced by the shaft bending stiffness. When the stiffness is low (high support stiffness), then the bearings and casing will strongly constrain the rotor motion at the bearings, and most of the vibration will occur through the bending of the shaft. Rotors which experience these shaft bending modes are called flexible rotors.

Flexible rotor balancing is much more complicated than the standard rigid rotor balancing techniques because the shape of the centroidal axis and the unbalance distribution changes with speed. Based on the complexity and the non-agreement with other balancing procedures flexible rotor balancing is known to be solved with three different techniques. The three techniques are modal balancing, influence coefficient balancing, and unified balancing approach [uba].

a. MODAL BALANCING

Modal balancing is based on assuming orthogonal modes of vibration deformation and tries to balance for these modal shapes. The minimum number of balance planes is equivalent to the number of vibrational modes. In today's world most machinery operates above the first balancing resonance, and many operate above the second mode (Vance,

1988). Machines with these multiple modes often require more complex balancing, where two or more planes are simultaneously balanced at one time.

In general, the deflection shape of a flexible rotor is the result of a combination of several modes of vibration. A rotor operating between resonances will usually have residual effects of the lower modes and at the same time the early effects of the higher modes. The first mode of a flexible rotor between the bearings is usually a simple, predominantly in-phase; bending mode with nodal point's inboard or outboard of the bearings (Darlow, 1987). The one exception to this rule is overhung rotors which ultimately have different mode shapes (Darlow, 1987). The second mode of flexible rotors is usually an out-of-phase bending mode. The deflection shape of this mode is S-shaped, with additional nodal points near the mid-span of the rotor (Vance, 1988).

The first mode will not respond to an out-of-phase unbalance distribution and the second mode will not respond to an in-phase unbalance distribution. Two identical weights have to be installed at the same angular location in both weight planes. This will cause the in-phase balancing force to actively affect the first mode, but will not excite the second mode. Similarly, if two identical weights are installed 180^o opposite each other in both weight planes, the out-of-phase balancing force created will excite the second mode, but will not excite the first mode. The ideal objective of modal balancing is to add weight in both planes so that both modes are balanced at once (Darlow, 1987).

The most general case of distributed unbalance u(z) may be expanded in terms of the modal eccentricity components in terms of the mode shapes.

$$u_{(Z)} = \sum F_k m_{(Z)} \Phi_k(z) \tag{3.24}$$

where F is the force, m is the mass, and Φ is the designated phase

$$u_1 = E_1 m_1 \Phi_{11} + E_2 m_2 \Phi_{21} \tag{3.25}$$

$$u_2 = E_1 m_2 \Phi_{12} + E_2 m_2 \Phi_{22} \tag{3.26}$$

$$u_3 = E_1 m_3 \Phi_{13} + E_2 m_2 \Phi_{23} \tag{3.27}$$

where m_i are masses at the balance stations. The effective masses may be computed from the critical speed mode shape and values of modal mass as follows:

$$M_1 = m_1 \Phi^2_{11} + m_2 \Phi^2_{12} + m_3 \Phi^2_{13} \tag{3.28}$$

$$M_2 = m_1 \Phi^2_{21} + m_2 \Phi^2_{22} + m_3 \Phi^2_{23} \tag{3.29}$$

The effective mass stations should also satisfy the rotor orthogonality conditions as follows:

$$0 = m_1 \Phi_{11} \Phi_{21} + m_2 \Phi_{12} \Phi_{22} + m_3 \Phi_{13} \Phi_{23} \tag{3.30}$$

The unbalance response can now be expressed as the sum of the modal components:

$$\begin{bmatrix} u_1 \\ u_2 \\ u_3 \end{bmatrix} = \begin{bmatrix} u_1 \\ u_2 \\ u_3 \end{bmatrix}_1 + \begin{bmatrix} u_1 \\ u_2 \\ u_3 \end{bmatrix}_2 \tag{3.31}$$

The first set of unbalances will excite the rotor first mode and the second set will only excite the second critical speed. The advantages of modal balancing are:

- The number of sensitivity runs at high speeds is minimized.
- Has very good sensitivity at high speeds.
- Balancing of a specific mode is permitted, while not affecting previously balanced modes.
- It can be an entirely empirical procedure.

b. INFLUENCE COEFFICIENT METHOD

Influence coefficient balancing is the determination of how a unit of unbalance at various mass locations along the z-axis is reduced by selecting discrete correction masses. These are used to minimize vibrational amplitudes at other locations along the same axis. In two plane balancing procedures, a trial weight is placed on the first or near the first plane and the according resultant measurements at the near and far planes are recorded. Based on these measurements, two influence coefficients are computed. The trial weight is then removed and placed at the second or far plane. Then the procedure is used to generate two more influence coefficients.

For illustrative purposes let $\{V_i\}$ be a column vector of I measured vibration phasors (amplitude and phase lag angle), $[C_{ij}]$ be the matrix of influence coefficients, and $\{U_j\}, \{M'_j\}, \{M_j\}$ be the column vectors, trial, and balance mass phasors, respectively.

$J = 2$ planes $(j = 1,2)$, $K = 2$ speeds, $L = 2$ transducers, so $I = 2 \times 2 = 4$ vibration measurements $(i = 1,2,3,4)$.

The original uncorrected rotor imbalance is given by:

$$\{V_i\} = [C_{i_j}]\{U_j\} \tag{3.32}$$

The component equations are:

$$V_1 = C_{11}U_1 + C_{12}U_2 \quad \text{(plane 1, speed 1);} \tag{3.33}$$

$$V_2 = C_{21}U_1 + C_{22}U_2 \quad \text{(plane 2, speed 1);} \tag{3.34}$$

$$V_3 = C_{31}U_1 + C_{32}U_2 \quad \text{(plane 1, speed 2);} \tag{3.35}$$

$$V_4 = C_{41}U_1 + C_{42}U_2 \quad \text{(plane 2, speed 2);} \tag{3.36}$$

The vibration produced by a set of trial masses $\{M'_j\}$ is:

$$\{V'_i\} = \{V_i\} + [C_{ij}]\{M'_j\} \tag{3.37}$$

Component equations for the special case are:

$$V'_1 = V_1 + C_{11}M'_1 + C_{12}M'_2 \tag{3.38}$$

$$V'_2 = V_2 + C_{21}M'_1 + C_{22}M'_2 \tag{3.39}$$

$$V'_3 = V_3 + C_{31}M'_1 + C_{32}M'_2 \tag{3.40}$$

$$V'_4 = V_4 + C_{41}M'_1 + C_{42}M'_2 \tag{3.41}$$

V'_i is measured with trial masses applied one at a time, the influence coefficients can be determined from the measurements. By way of example the equation:

$$V'_4 = V_4 + C_{41}M'_1 + C_{42}M'_2 \tag{3.42}$$

Gives the vibration in plane 2 at speed 2 with trial masses M'_1 attached as:

$$V'_{41} = V_4 + C_{41}M'_1 \tag{3.43}$$

This allows C41 to be calculated as:

$$C_{41} = \frac{V'_{41} - V_4}{M'_i} \tag{3.44}$$

The advantages of the influence coefficient method are:

- It is an entirely empirical procedure which requires minimal prior knowledge.
- Full sensitivity information allows convenient balancing of any combination of critical speeds.
- It is readily computerized and automated.
- It provides for least-squares minimization of data from any number of vibration sensors.

c. UNIFIED BALANCING APPROACH

Unified approach is considered a combination of modal and influence coefficient balancing. It applies the theoretical approach of influence coefficient while taking advantage of the modal behavior of the rotor. This process incorporates the advantages of both modal and influence coefficient, while eliminating the disadvantages of both methods. In the case of the unified approach balancing near the first or higher order critical speed, a modal unbalance distribution is used rather than a single value. The trial unbalance distribution for the first mode is given by:

$$[u_1]_T = u_T \begin{bmatrix} 1 \\ \frac{m_2\Phi_{12}}{m_1\Phi_{11}} \\ \frac{m_2\Phi_{12}}{m_1\Phi_{11}} \end{bmatrix} \tag{3.45}$$

where $\Phi_{12,}\ \Phi_{11,}\ \Phi_{13}$ are the phase locations. This trial weight distribution is placed on the shaft and the rotor amplitude is measured. The trial unbalance eccentricity is given by:

$$E_{1t} = \frac{u_T}{M_1}\left[\Phi_{11} + \frac{m_2\Phi^2{}_{12}}{m_1\Phi_{11}} + \frac{m_3\Phi^2{}_{13}}{m_1\Phi_{11}}\right] \tag{3.46}$$

The rotor amplitude of motion at any point along the rotor is given by:

$$[y]_T = (E_1 + E_{1T})A_1[\Phi_1] + E_2A_2[\Phi_2] + \ldots + E_jA_j[\Phi_j] \tag{3.47}$$

Subtracting the original measured amplitude at station k from the trial run we obtain:

$$y_{Tk} - y_k = E_{1T}A_1\Phi_{k1} \tag{3.48}$$

The complex first modal amplification factor is determined by:

$$A_1 = \frac{1}{N}\sum^{N}\left(\frac{y_{Tk} - y_k}{E_{1T}\Phi_{ik}}\right) \tag{3.49}$$

where N is the number of stations at which measurements are made. If the first probe is assumed to be near the maximum rotor amplitude then the modal unbalance is given by:

$$E_1 = \frac{y_1}{A_1\Phi_{11}} = \left(\frac{y_1}{y_{T1} - y_1}\right)E_{1T} \tag{3.50}$$

The modal balance correction E_{1b} is placed opposite the unbalance eccentricity:

$$E_{1b} = -E_1$$

The correction balance weights for the first critical speed are simply given by ratio of rotor amplitude at the center station 1 by:

$$\begin{bmatrix} u_{11} \\ u_{21} \\ u_{31} \end{bmatrix}_b = \left(\frac{y_1}{y_1 - y_{T1}}\right)\begin{bmatrix} u_{11} \\ u_{21} \\ u_{31} \end{bmatrix}_T \tag{3.51}$$

CHAPTER IV

BALANCING OF A ROTOR TEST RIG RK-4

A. DESCRIPTION OF RK-4

The Bently Nevada Corporation (BNC) RK-4 test rig is a unique laboratory tool based upon its exclusive geometry and its capability to isolate and control any particular individual machine characteristics. These distinctive abilities make it an exceptional candidate for both a teaching tool and for theoretical rotordynamic research. The RK-4 test rig can be used for, but not limited to the following:

- Rotor unbalance – single and multi-plane
- Shaft rub conditions
- Oil whirl and oil whip instabilities
- Shaft perturbation
- Others

The RK-4 test rig has a V – frame design which helps reduce housing dynamic stiffness properties because the mechanical tolerances have been tightened to ultimately improve the machine behavior modeling. The RK-4 holds the desired speed with ease while loading conditions are changed based upon the direct current motor and the high performance control.

Figure 11: RK 4 Tested Configuration

Figure 11 above represents the tested rotor kit which was composed of the following:

- Motor
- Motor Speed Controller
- Shaft
- Two bearings
- Two disks
- Two X-Y Mounts
- Four probes
- One keyphasor probe
- One RPM probe
- Mounting plate
- Three safety covers

The Automated Diagnostics for Rotating Equipment (ADRE) data acquisition software and a PC can be used for all of the data manipulation. The ADRE software is a powerful tool which provides real-time signal processing. This software has extensive capabilities in plotting, import/export, and rotating machinery balancing. What makes the ADRE software so nice is the fact that it is fully integrated with Bently BALANCE, which is the industries most powerful multi-plane balancing software. The ADRE data acquisition device is also capable of allowing several probes to be hooked up at one time. Figure 12 below identifies al of the probes in the tested configuration.

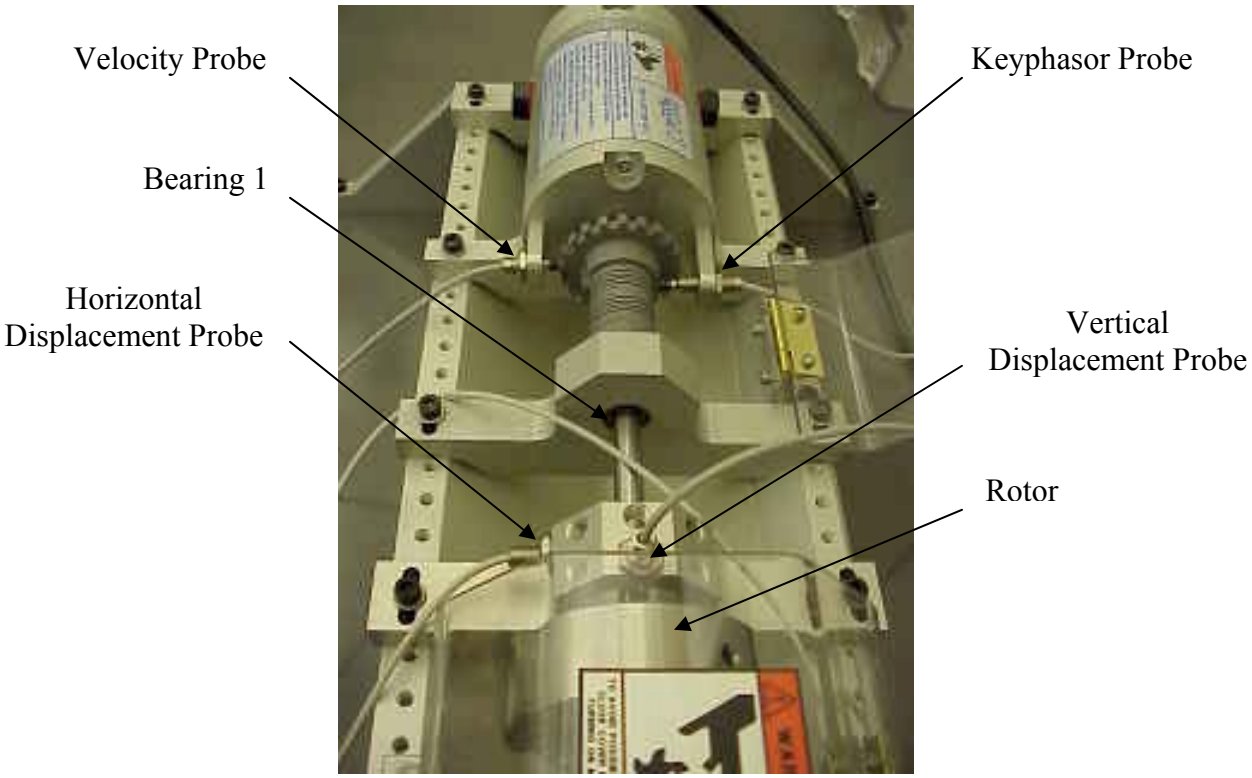

Figure 12: Probe Setup

All of the probes listed above can be plugged into the designated spots and positions on the back of the ADRE data acquisition system. The vertical probe can be plugged into probe 1 input while the horizontal probe can be plugged into probe 2. The other probe block is not shown for the sake of simplicity but, the vertical probe of that

assembly is plugged into probe 3 and the horizontal probe is plugged into probe 4. These probes can be mounted on the probe block and the probe block should be placed less than one inch in front of or behind the rotating disks.

The gap between these probes and the shaft can be determined by reading the voltage. The proper placement of the proximity probes should be set to the manufacturer's guidelines based on the transducer size and their linear range. Based on the proximity probes that were used the manufacturer required a voltage reading equal to -8V ± 0.5V. Setting the probe to the recommended specification for the probe would ensure that the proximity probe was set at the center of its linear range to maximize reading of the vibration signal. Setting it at the required voltage would also help to ensure that there was more than enough clearance between the probe and the rotating shaft.

The keyphasor alignment probe is a little more complicated in its setup. The voltage of the keyphasor probe should be -5V ± 0.5V. The keyphasor probe must be setup in accordance with the rotating mass so that angular placement is set. The system should be setup to rotate counterclockwise when viewed from the motor looking towards the mass. Rotate the system in that direction until the leading edge of the keyphasor notch is lined up with the center of the keyphasor probe. Then align the 0^{o} mark on the mass with the keyphasor probe which is shown in figure 13 below.

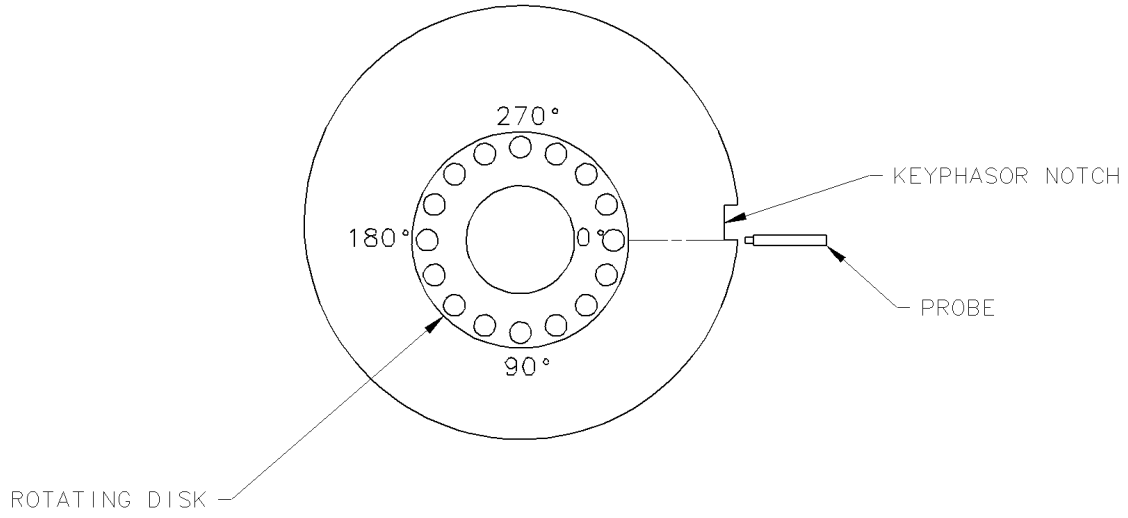

Figure 13: Rotor Angular Positioning

B. ROTOR CONFIGURATION AND ROTORDYNAMIC ANALYSIS

Many different disk/bearing combinations can be evaluated with the rotor kit. A two-disk, two-bearing combination was modeled in this experiment. Figure 14 depicts the configuration of the test setup. The bearings were placed at the beginning and end of the shaft. Both disks were positioned between the two bearings 25% and 75% of the total span of the shaft. All relative dimensions for the configuration have been provided in figure 15 while figure 16 provides an isometric viewpoint.

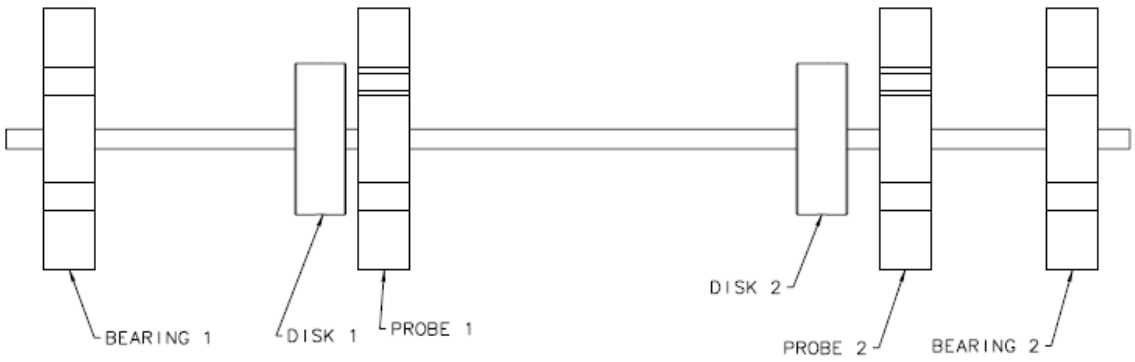

Figure 14: Labeling of Rotor Test Components

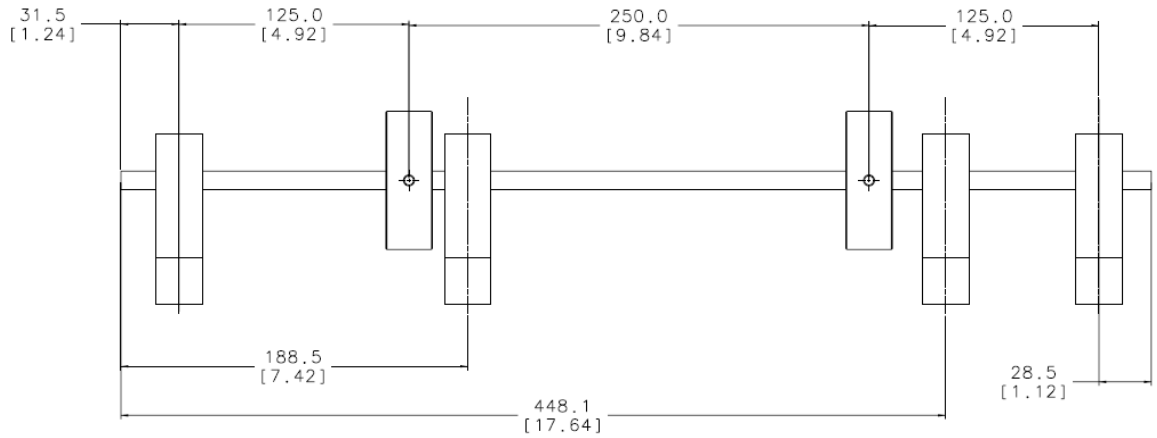

Figure 15: Precise Placement of Rotor Components

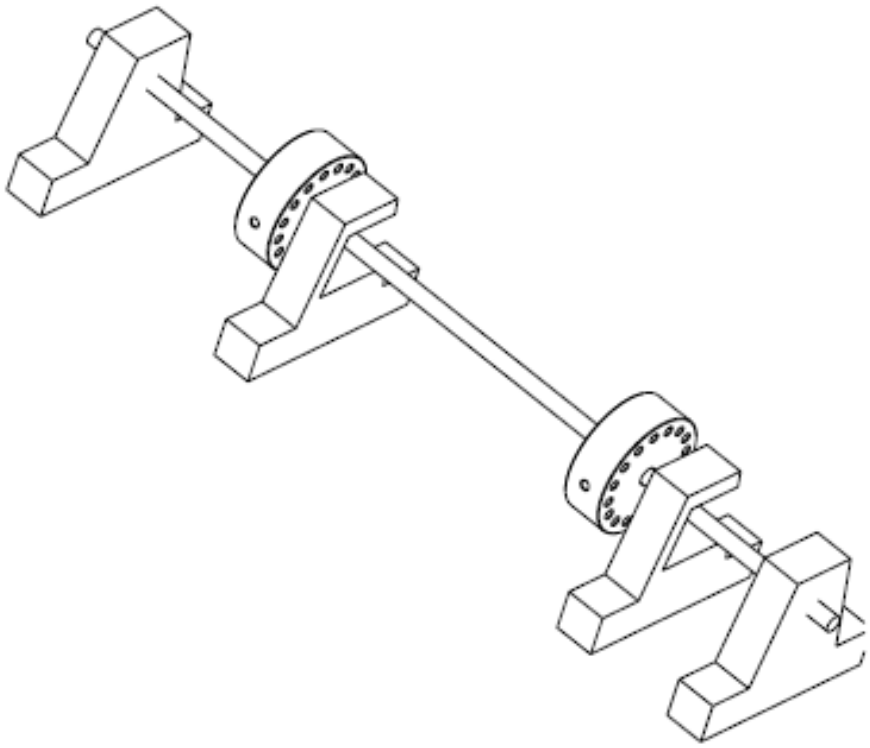

Figure 16: Isometric View of the Rotor Rig

The extensive arrangement of the tested configuration was the lengthiest aspect of the entire process. Accurately locating and measuring the rotating disks were a crucial step in finding the modes and critical speeds. After this initial setup of the configuration was complete the adjusted density of the rotating disks was needed in order to perform a

proper rotordynamic analysis on the configuration. There are many holes in the rotating disk and because of these holes the adjusted density of the disk is different than the density of mild carbon steel. The density of mild carbon steel is 0.283 lb/in^3. The adjusted density of the disk was calculated to be 0.255 lb/in^3. This adjusted density is very critical in order to get the proper calculations. The rotordynamic analysis program is very sensitive to the density of the rotating disk. The more accurate the density calculation of the disk is the better the results will be for the mode shapes and critical speeds. The calculation for the adjusted density of the disk is below.

Carbon Steel Density and Modulus of Elasticity:

$$\rho = 7861.093 \frac{Kg}{m^3}$$

$$E = 2.068 \times 10^{11} Pa$$

Volume of the Disk:

$$V = \pi r^2 l = \pi \left(\frac{0.0755}{2} \right)^2 (0.0254) = 1.137 \times 10^{-4} \ \text{m}^3 \qquad (4.1)$$

where r is the radius and l is the thickness.

Mass of Disk:

$$m = \rho V = 7861.093 \times \left(1.137 \times 10^{-4}\right) = 0.894 \ \text{Kg} \qquad (4.2)$$

where ρ is the density and V is the volume.

Based on the fact that there are 16 – 5mm holes around the circumference of the disk, 1 – 5mm hole radially, and 1 – 10mm hole through the center of the disk a correction for the disk density has to be done.

16 holes with Ø = 5 (mm):

$$V = \pi r^2 l = \pi\left(\frac{0.005}{2}\right)^2 (0.0254) = 4.987\times10^{-7} \ \text{m}^3 \tag{4.3}$$

$$m = \rho V = 7861.093\times\left(4.987\times10^{-7}\right) = 0.004 \ \text{Kg} \tag{4.4}$$

$$m_{16} = m\times16 = 0.004\times16 = 0.063 \ \text{Kg} \tag{4.5}$$

1 hole with Ø = 5 (mm):

$$V = \pi r^2 l = \pi\left(\frac{0.005}{2}\right)^2 (0.0755) = 1.473\times10^{-6} \ \text{m}^3 \tag{4.6}$$

$$m = \rho V = 7861.093\times\left(1.473\times10^{-6}\right) = 0.012 \ \text{Kg} \tag{4.7}$$

1 hole with Ø = 10 (mm):

$$V = \pi r^2 l = \pi\left(\frac{0.01}{2}\right)^2 (0.0254) = 1.995\times10^{-6} \ \text{m}^3 \tag{4.8}$$

$$m = \rho V = 7861.093\times\left(1.995\times10^{-6}\right) = 0.016 \ \text{Kg} \tag{4.9}$$

Total Mass of Disk:

$$m_{disk} = 0.894 - 0.063 - 0.016 - 0.012 = 0.803 \ \text{Kg} \tag{4.10}$$

Disk Density Correction:

$$\rho_{disk} = \frac{m_{disk}}{V} = \frac{0.803}{1.137\times10^{-4}} = 7062.445\frac{Kg}{m^3} \tag{4.11}$$

Once the required measurements were taken and the adjusted densities of the disks were found all of the data was used in the Rotor Critical Speed Analysis Program. This program made it quite simple to do the rotordynamic analysis of the tested configuration. The tables 1 – 3 below show the data that was input into the program. Figure 17 below shows how the rotor configuration was cut into pieces for the rotordynamic analysis.

Station #	Disc Weight (Lb)	Disc Diameter (in)	Disc Thickness (in)	Disc Density (Lb/in^3)	Polar Moment (Lb-In^2)	Trans Moment (Lb-In^2)	Disc Orientation
7	1.54	2.95	0.9	2.55E-01	1.71	9.60E-01	Centered
18	1.54	2.95	0.9	2.55E-01	1.71	9.60E-01	Centered

Table 1: Disc Input Data

Station #	Station Length (in)	Station Weight (lb)	External Diameter (in)	Station Density (lb-in^3)	EI (lb-in^2)	Polar Moment (lb-in^2)	Trans Moment (lb-in^2)	Z Position (in)
1	1.24	0.02	0.41	2.83E-01	4.37E+04	1.71	9.64E-01	0.0
2	0.98	0.04	0.41	2.83E-01	4.37E+04	1.71	9.64E-01	1.2
3	0.98	0.04	0.41	2.83E-01	4.37E+04	1.71	9.64E-01	2.2
4	0.98	0.04	0.41	2.83E-01	4.37E+04	1.71	9.64E-01	3.2
5	0.98	0.04	0.41	2.83E-01	4.37E+04	1.71	9.64E-01	4.2
6	0.98	0.04	0.41	2.83E-01	4.37E+04	1.71	9.64E-01	5.2
7	0.98	1.58	0.41	2.83E-01	4.37E+04	1.71	9.64E-01	6.2
8	0.98	0.04	0.41	2.83E-01	4.37E+04	1.71	9.64E-01	7.1
9	0.98	0.04	0.41	2.83E-01	4.37E+04	1.71	9.64E-01	8.1
10	0.98	0.04	0.41	2.83E-01	4.37E+04	1.71	9.64E-01	9.1
11	0.98	0.04	0.41	2.83E-01	4.37E+04	1.71	9.64E-01	10.1
12	0.98	0.04	0.41	2.83E-01	4.37E+04	1.71	9.64E-01	11.1
13	0.98	0.04	0.41	2.83E-01	4.37E+04	1.71	9.64E-01	12.1
14	0.98	0.04	0.41	2.83E-01	4.37E+04	1.71	9.64E-01	13.0
15	0.98	0.04	0.41	2.83E-01	4.37E+04	1.71	9.64E-01	14.0
16	0.98	0.04	0.41	2.83E-01	4.37E+04	1.71	9.64E-01	15.0
17	0.98	0.04	0.41	2.83E-01	4.37E+04	1.71	9.64E-01	16.0
18	0.98	1.58	0.41	2.83E-01	4.37E+04	1.71	9.64E-01	17.0
19	0.98	0.04	0.41	2.83E-01	4.37E+04	1.71	9.64E-01	18.0
20	0.98	0.04	0.41	2.83E-01	4.37E+04	1.71	9.64E-01	19.0
21	0.98	0.04	0.41	2.83E-01	4.37E+04	1.71	9.64E-01	19.9
22	0.98	0.04	0.41	2.83E-01	4.37E+04	1.71	9.64E-01	20.9
23	1.12	0.04	0.41	2.83E-01	4.37E+04	1.71	9.64E-01	21.9
24	0	0.02	0.41	2.83E-01	4.37E+04	1.71	9.64E-01	23.0

Table 2: Complete Rotor Model Data

Station #	Stiffness (Lb/in)
2	850
23	850

Table 3: Bearing Data

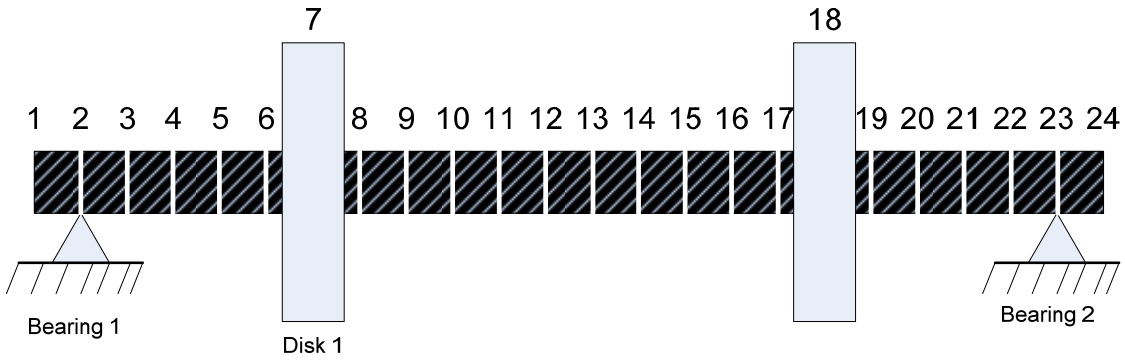

Figure 17: Complete Rotor Station Layout

The program was set up to calculate the first five fundamental frequencies in the rotating system as well as give the mode shapes of each resonance. Based upon the measurements and the given data of the system there were two modes shapes that were found in the tested configuration. The first and second mode shapes are displayed below in figure 18. This figure shows how the shaft will deform when the assembly spins through the first and second critical speeds. Mode 1 is at a speed of 1894 RPM while the second mode is around 4775 RPM.

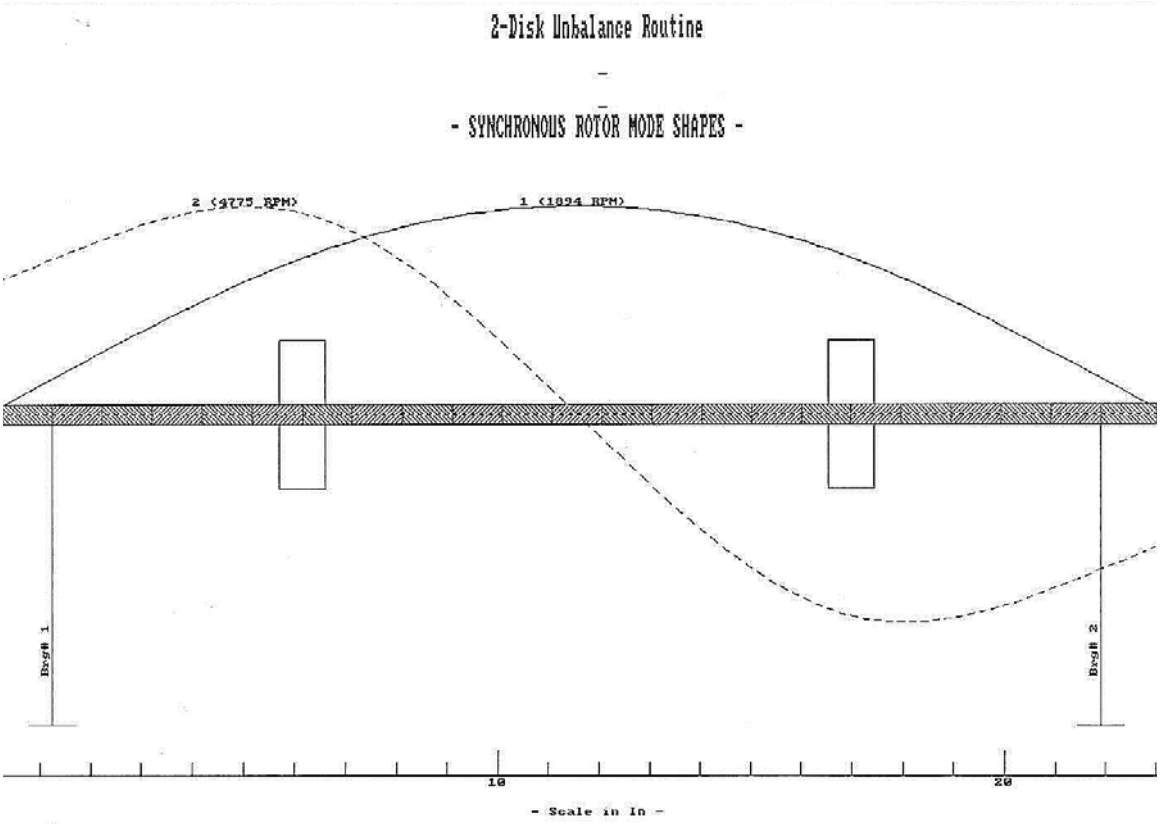

Figure 18: Mode Shapes at the First Two Critical Speeds

The first mode of vibration was the only frequency analyzed in this experiment for simplification. In order to confirm that the data, which was entered into the program for the initial rotor analysis was correct, a preliminary spin up of the assembly was

performed. After the initial spin-up of the rotor was completed an accurate and more reliable resonance was found. The discovered resonance was around 1915 RPM. This frequency of 1915 RPM helps to solidify the preliminary rotordynamic calculations done by the critical speed program. The original calculations of the first critical speed 1894.29 RPM were considered to be quite accurate and provided a reliable starting point for the analysis. Table 4 shows the first two resonance frequencies of the tested configuration.

Mode #	RPM	Hz
1	1894.29	31.57
2	4774.65	79.58

Table 4: Two Modes Found in Tested Configuration

C. ROTOR BALANCING USING INFLUENCE COEFFICIENT METHOD

Based on the rotor spin-up and the rotordynamic analysis the rotor was ready to be balanced using the influence coefficient method. The first step in the experiment consisted of balancing the rotor, as precisely as possible, over the desired speed range. The desired speed range for the system was 300 RPM to 2,500 RPM. Trial runs were completed at the desired speed range in order to assist in making sure that the ADRE Data acquisition software was plotting and recording the pertinent information for the experiment. The first orbital plots from the spin-ups are shown in the figures 19 and 20 below.

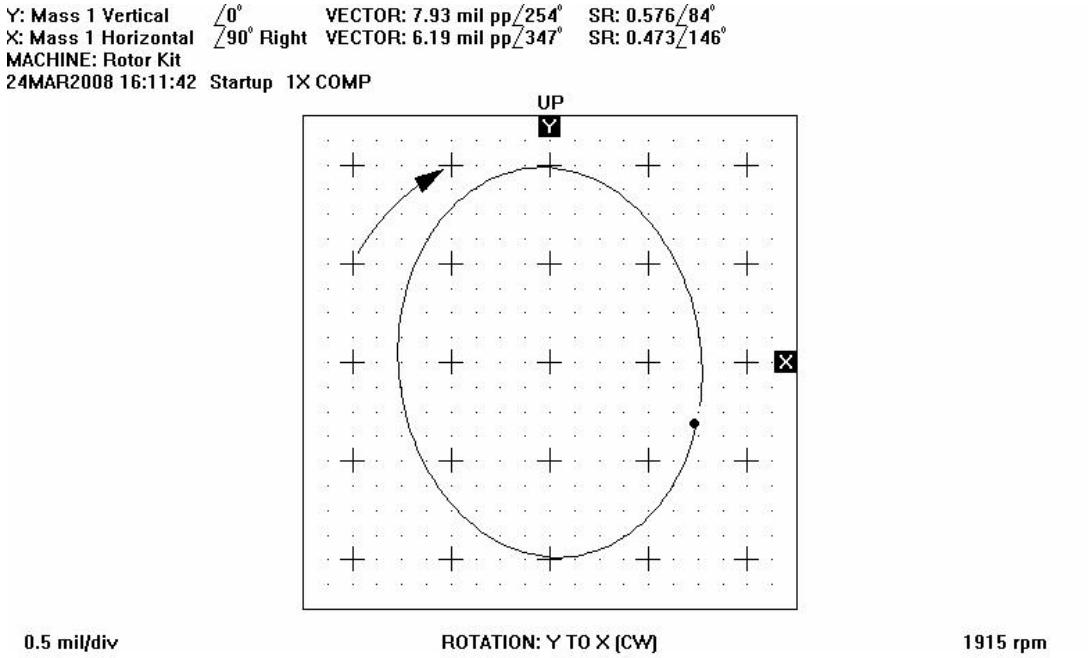

Figure 19: Disk 1 Unbalanced Orbit

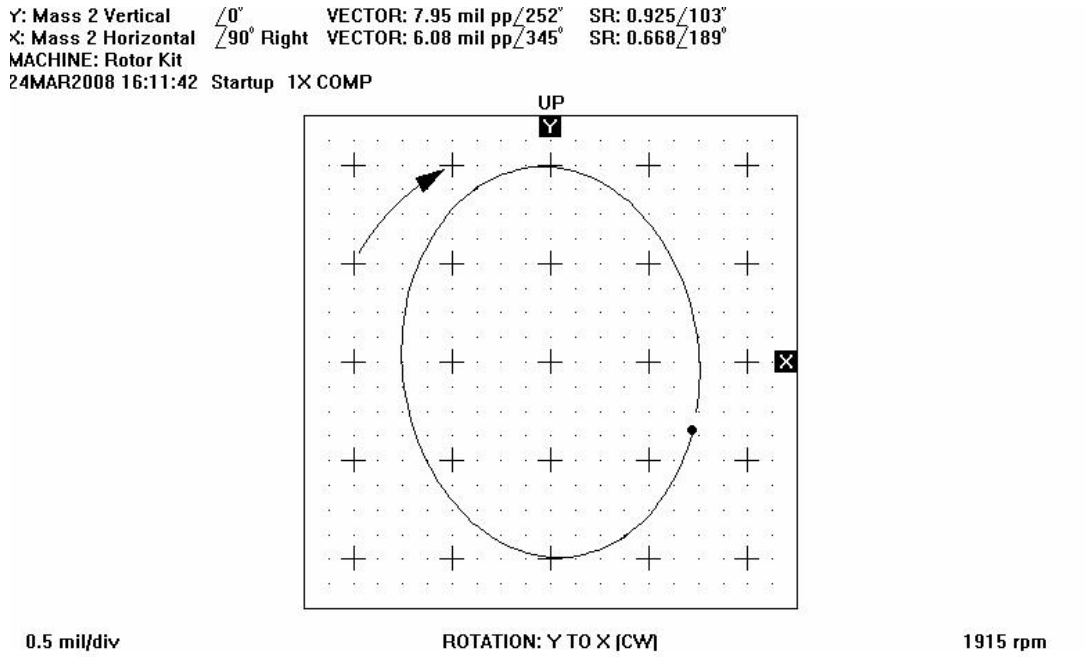

Figure 20: Disk 2 Unbalanced Orbit

After the first resonance was observed and the data was collected for the unbalance response another run was performed of the rotor assembly. This run consisted of adding a trial weight to the two rotors at a specified angle and collecting the data at the

resonant speed of 1915 RPM. The weight configuration used was a 0.2 g balance shot which was located at the 0^{o} mark on each rotor. The trial weight was installed at the specified location on mass 1 and the rotor was spun to the resonant frequency and the plots were recorded. The weight was removed from the first disk and placed on the second disk at the same specified location and again the rotor was spun to the resonant frequency and the data and plots were recorded. These plots of the amplitude and phase data are shown below in figure 21 - 24.

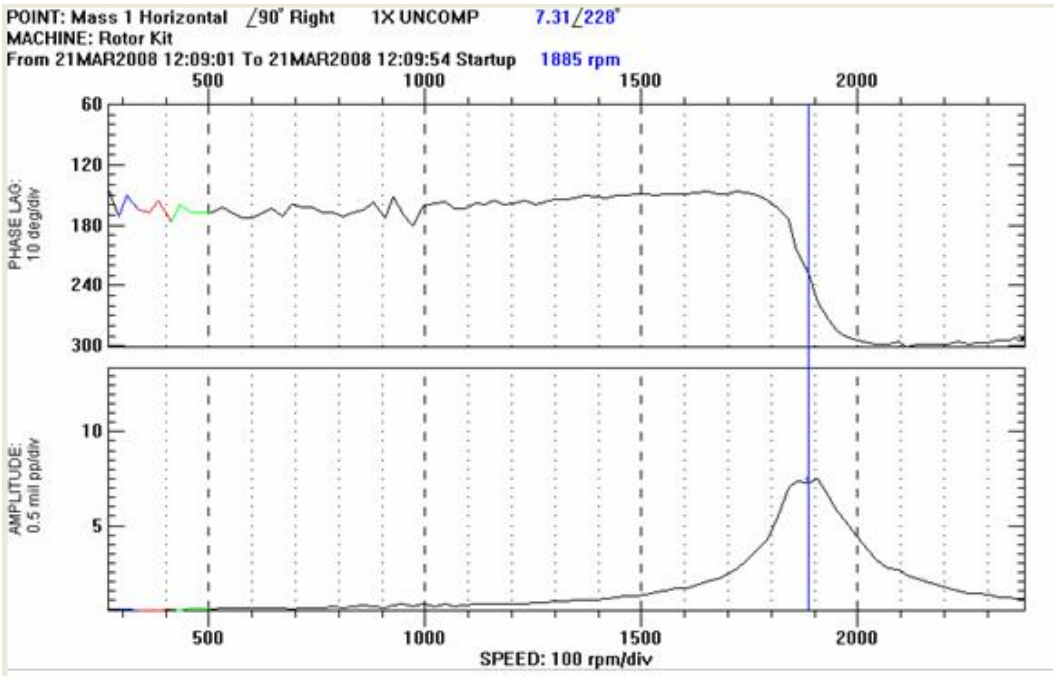

Figure 21: 0.2g Response Disk 1 Horizontal Probe

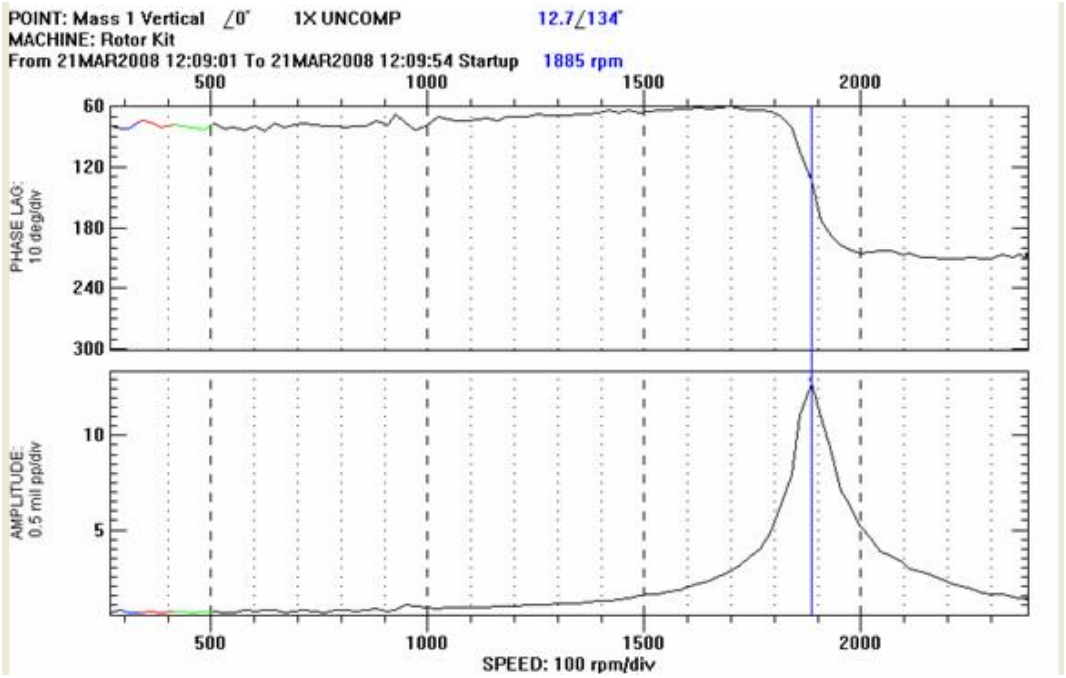

Figure 22: 0.2g Response Disk 1 Vertical Probe

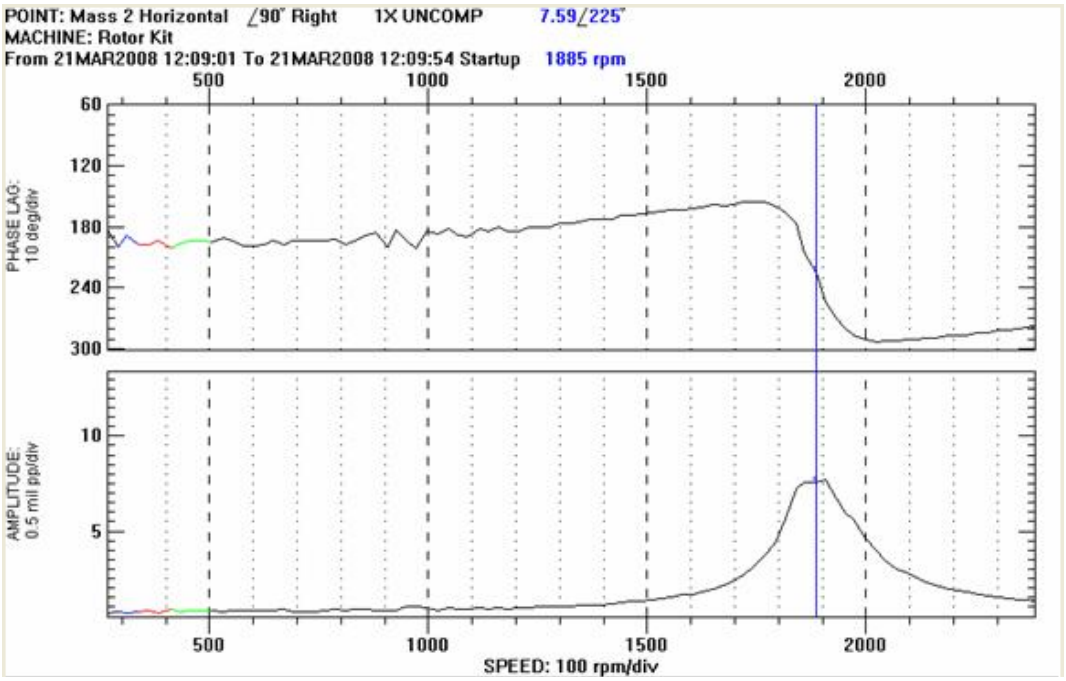

Figure 23: 0.2g Response Disk 2 Horizontal Probe

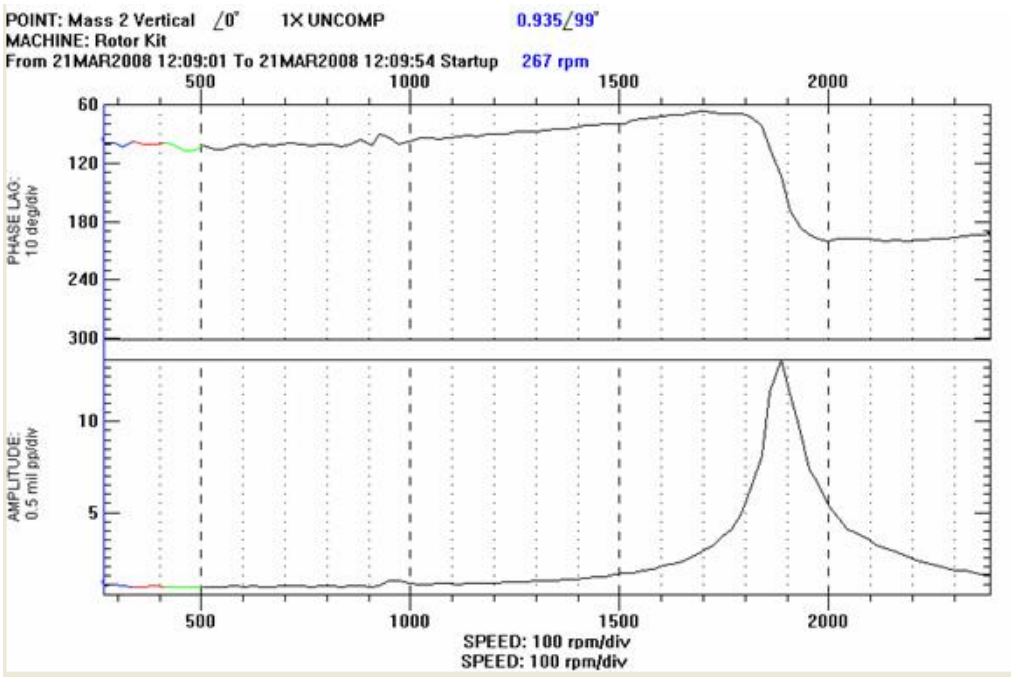

Figure 24: 0.2g Response Disk 2 Vertical Probe

The program Flexbal.exe (Adams, 2000), which was written by David Fleming, was utilized to determine the magnitude and the location of the weights required to balance the rotor. The amplitude and phase data collected during the first part of the experiment was entered into the program. The program provided the mass and location of the counter balance weights that needed to be added to the rotating system in order to achieve the best balance possible. It is necessary to vectorially manipulate the output from the balancing program in order to apply it to the tested configuration. This occurs because there are a limited number of holes in each rotating disk where the balancing weights can be added. The holes are evenly distributed radially, and are located in increments of 22.5^{o} around the disk. The balancing program also provides residual vibration, which is still present after balancing. The residual vibrations from the program are documented in table 5.

Probe	Speed (RPM)	Amplitude (mils)	Phase (degree)	Amplitude (mils)	Phase (degree)	Amplitude (mils)	Phase (degree)
1	1912	0.813E -07	29.2	0.813E -07	29.2	0.813E -07	29.2
2	1912	4.83E-07	95.4	4.83E-07	95.4	4.83E-07	95.4

Table 5: Residual Vibration after Balancing

The program defined the balance weights to be 0.1241g @ 39.7^o for mass 1 and 0.1084 g @ 253.7^o for mass 2. The first mass angular location is between 22.5^o and 45^o while the second mass location is between 247.5^o and 270^o. There is no weight positioning hole at these specified locations, the weight was distributed proportionally among the adjacent holes which can be seen in figure 25.

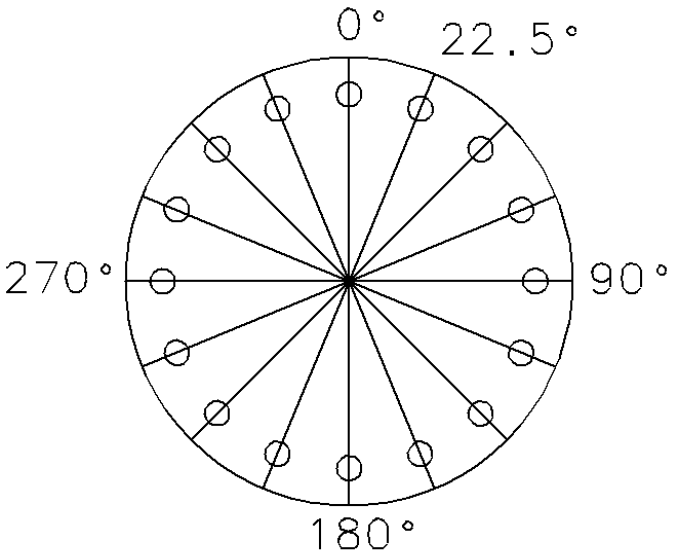

Figure 25: Weight Position Reference

Mass 1: Weight distribution calculation.

The weight location was calculated to be 39.7^o. The closest weight locations on the disk are considered to be 22.5^o and 45^o respectively. Based on the fact that the weight stations are 22.5^o apart the following ratio can be set up:

$$\frac{45^\circ - 22.5^\circ}{45^\circ - 39.7^\circ} = \frac{22.5^\circ}{x} \tag{4.12}$$

Solving for x in this ratio:

$$22.5x = 119.25 \tag{4.13}$$

$$x = 5.3^{\circ} \text{ in plane 1 (mass 1)} \tag{4.14}$$

Subtracting x from the weight incremental location of 22.5^{o} renders:

$$y = 22.5 - 5.3 = 17.2^{\circ} \tag{4.15}$$

From this angle the following trigonometric equation can be stated below:

$$A\cos(x) + B\cos(y) = imbalance \tag{4.16}$$

Substituting the variables into equation 4.16 result in:

$$A\cos(5.3^{\circ}) + B\cos(17.2^{\circ}) = 0.1241 \tag{4.17}$$

Setting up an alternate equation based on the sine component of the vectors results in:

$$A\sin(5.3^{\circ}) = B\sin(17.2^{\circ}) \tag{4.18}$$

Solving for A in equation 4.18 gives:

$$A = B\left(\frac{0.29571}{0.924}\right) \tag{4.19}$$

Further reducing equation 4.19:

$$A = B(3.20) \tag{4.20}$$

Substituting equation 4.20 into equation 4.17:

$$B(3.2)\cos(5.3^{\circ}) + B\cos(17.2^{\circ}) = 0.1241 \tag{4.21}$$

Combining like terms in equation 4.21:

$$3.186B + .956B = 0.1241 \tag{4.22}$$

Solving equation 4.22 for B:

$$B = 0.03\,\text{g} \text{ @ } 22.5^{o} \tag{4.23}$$

Plugging the answer B from equation 4.23 into 4.20 results in the answer for A:

$$A = 0.1 \text{ @ } 45^{o} \tag{4.24}$$

The same process can be applied to the second disk in order to calculate the distributed mass. These calculated masses are shown below.

Mass 2: Weight distribution calculation.

$$B = 0.08 \text{ g @ } 270^{o}$$

$$A = 0.03 \text{ g } 247.5^{o}$$

Data was able to be compiled and recoded by strategically placing the specified weights at there target locations and spinning the rotor configuration up to the resonant speed. Figure 26 and 27 below revealed a decrease in the mils values for the amplitudes as compared to the original unbalanced orbit plots.

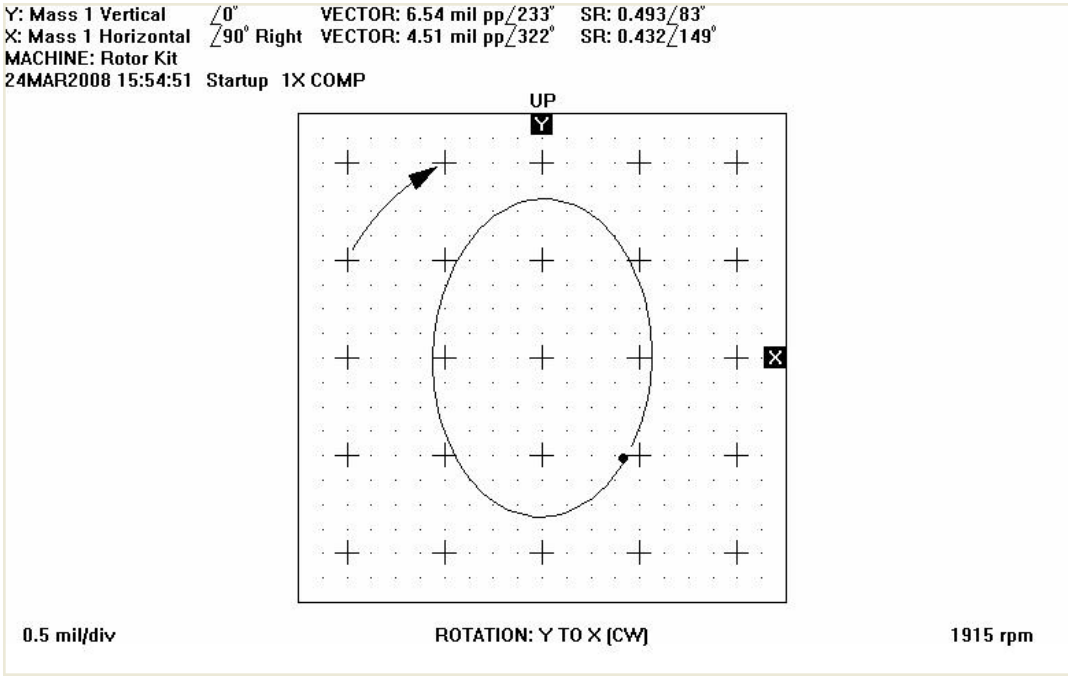

Figure 26: Balanced Disk One Orbit

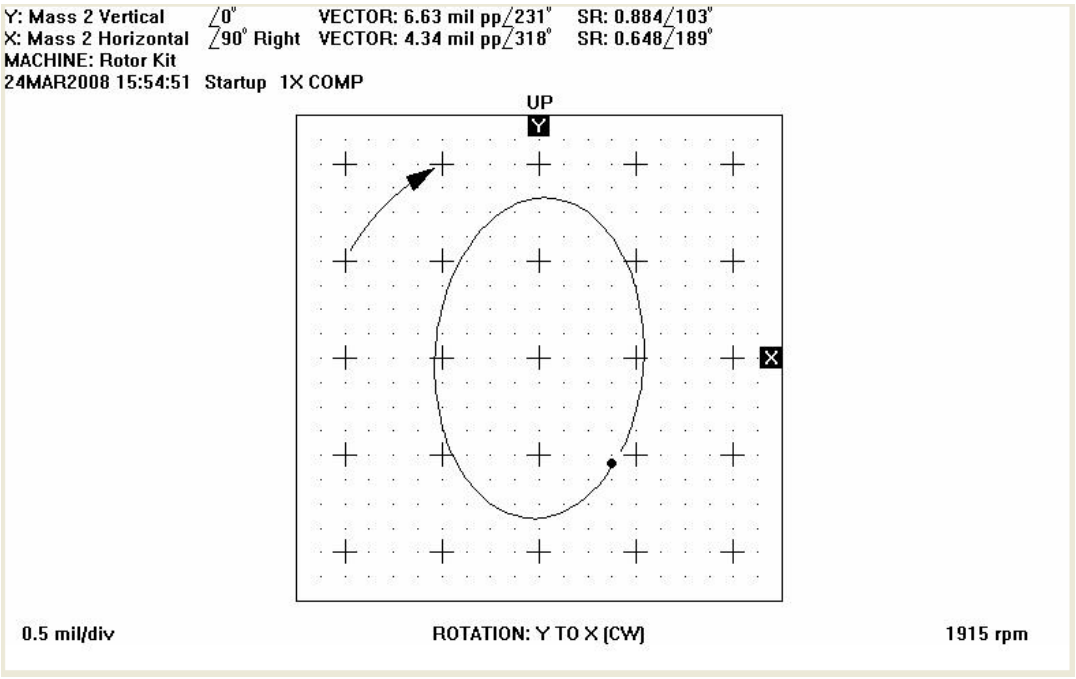

Figure 27: Balanced Disk Two Orbit

D. RESULTS AND CONCLUSIONS

Based upon the tested configuration above the experiment went well in its fundamental approach. The technique used to initially start the rotordynamic analysis was extensively time consuming. Although for any experiment the setup time is the most crucial portion. The reason for this initial setup complexity was largely due to my inexperience with the rotor test rig.

The concluding results show that the balancing of the disk did reduce the magnitude on the orbital plots with the introduction of the specified counterbalance weights. The required correction weights are defined in table 6.

CORRECTION WEIGHTS				
PLANE	WEIGHT (gram)	ANGLE (Deg)	X COMPONENT (mm)	Y COMPONENT (mm)
1	0.1241	39.7	9.553E-02	7.922E-02
2	0.1084	253.7	-3.041E-02	-0.1041

Table 6: Balance Weight Locations

Once these balance weights were added to the rotor the final balance orbits were recorded. These plots can be seen in figures 26 and 27 shown above. From the original rotor response which can be seen in figures 19 and 20. The data that was collected showed that the imbalance amplitudes did decrease after the balance weights were added to the disks.

The original imbalance of the disk was still within the desired operating tolerances of the system. Balancing the disk had no significant value to the rotor configuration or the operation. Even though it did not have a significant impact on the rotor configuration it did play a significant part in the understanding of how influence coefficient method works on rotating machinery. This experiment proved to be a success and also had many influential aspects that generated further curiosity. Through theory it is possible for one to inherently grasp an understanding of rotordynamics but through practice one can fully comprehend the intrinsic complexity of the process.

CHAPTER V

CASE STUDY: PHILIPS CT SCANNER

Based on the complexity and detail involved with balancing a CT scanner many techniques are used when a new product introduction is slated. Rigid rotor balancing techniques are used throughout the design phase of the product. This is largely due to the speed of the rotating array. The CT scanner rotor operates at a speed range more than 20% below the resonant frequency of the entire system. The operating frequency is 3.67 Hz while the first critical speed is around 8 Hz. Because of this aspect flexible rotor techniques are very hard to employ on the scanner.

The other major contributor which makes it difficult to balance the rotor is the complexity of the data acquisition placement. There are only a few places that acquisition devices can be implemented in order to collect data from the rotor. The rotor itself is very tough to access because of the ducting and other seal rings which are installed around the rotating array. Trying to implement the rotor with measurement devices is a process that can not be done smoothly or quickly.

Early in the design process CG locations of each individual rotating mass on the rotor are inserted into a special Matlab code. The program output not only theoretically balances the rotating array but it also specifies a weight configuration and shows where

counterbalance locations need to be on the array. Upon completion of this program the initial weight configuration and locations will be implemented into the design process.

Once the rotor has been optimized for the weight locations then the dynamic rigid rotor techniques are employed. This is done in order to fine tune the balance weights and lower the vibrational amplitudes for a clinical image quality. There are strict standards for the motion allowed at the iso-center plane of the system in order to get the best clinical images. The smaller amount of motion that iso-center experiences the sharper the image quality will be for the end user.

A. DESCRIPTION OF TEST SCANNER

The test scanner is a prototype with the same rotating array as on the released product line. It has all of the components that are installed on a production unit and the masses of the components are assembled in the exact same way. The rotating array weighs 1266 Kg and has an inertia of 600 Kg-m^2. The rotating array rotates in a clockwise rotation at an optimum balancing speed of 120 rpm, which is well below the critical speed of the system. The maximum operating rotational speed is 220 RPM (3.67 Hz) while the first natural frequency is around 8 Hz. Rigid rotor techniques are used to analyze the rotating array based on the fact that the system can not go up to the critical speed. Figure 28 below describes how masses are distributed on the rotating array.

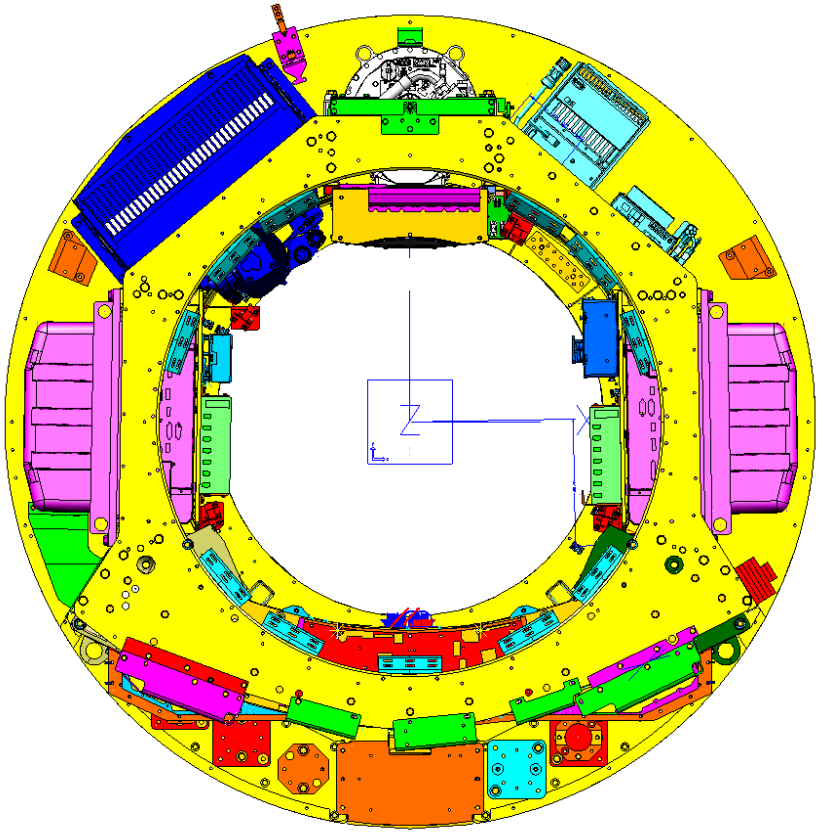

Figure 28: Distributed Mass on the Rotating Array

The other problem which arises from this configuration is the overhung load of the rotor. The main bearing in the system is far back in the Z-direction. In order to keep the rotor loading out of the bearing (distortions) there is isolation coil (Nest of Springs) which attaches the rotor to the bearing. This isolation coil subsides the axial and radial loading to the bearing and holds the entire translated rotor loading within the assembly. All of these entities are marked in figure 29 below.

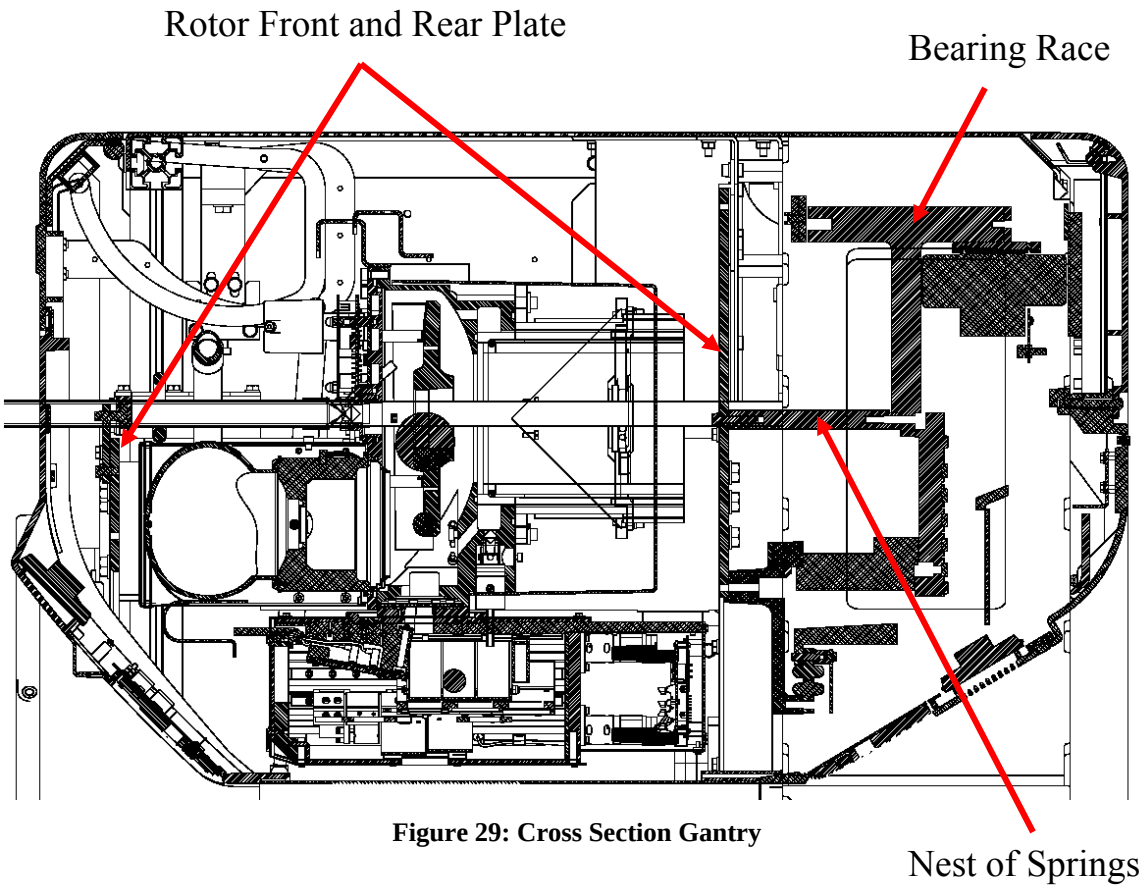

Figure 29: Cross Section Gantry

Ultimately this turns balancing the CT scanner rotor into a unique and iterative process. The rotor is attached to the tilting stator portion of the scanner. The tilt frame can be seen in figure 30. These two components are attached at a pivot position to the column assembly which can be seen in figure 31.

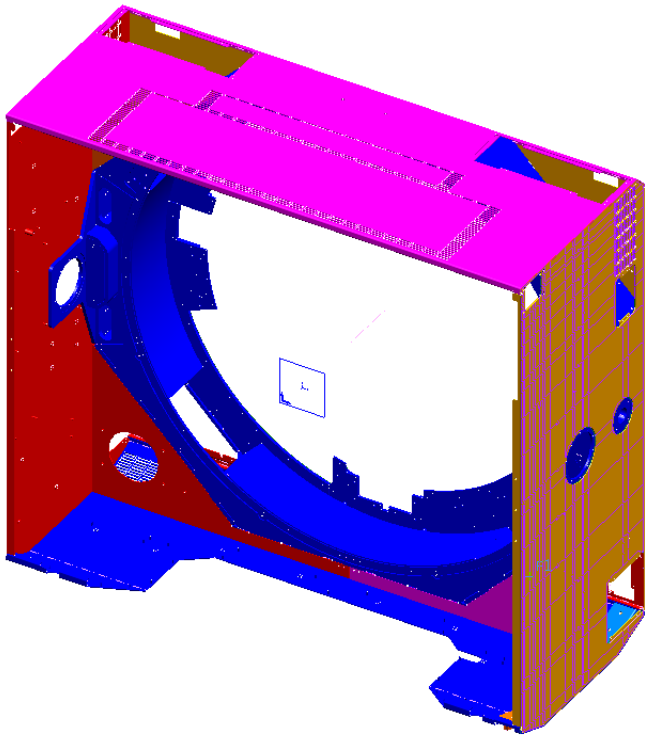

Figure 30: Tilt Frame Assembly

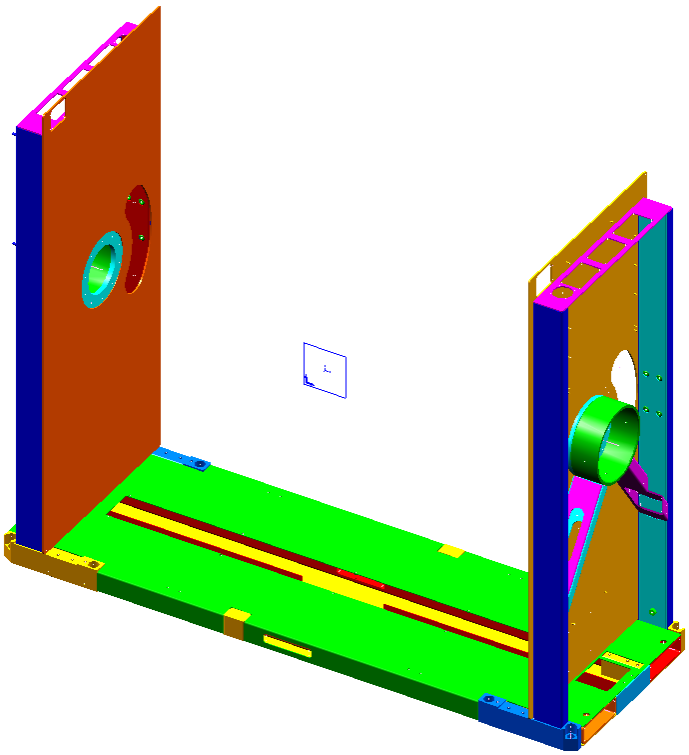

Figure 31: Column Assembly

The tilting stator portion of the scanner is rotated about a pivot point which is completed via a pivot shaft and spherical bearing. Figure 32 is a representation of the spherical bearing in the system while figure 33 shows all technical data.

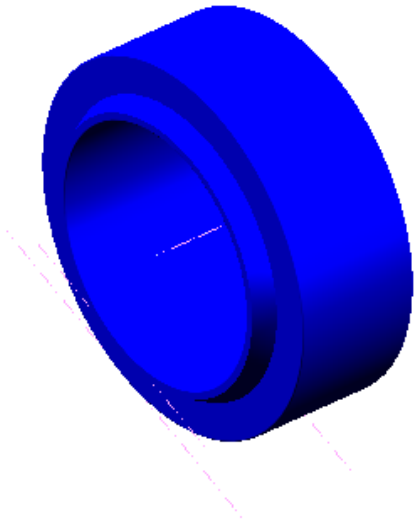

Figure 32: Pivot Bearing

Maintenance-free radial spherical plain bearings

Tolerances , see also text
Radial internal clearance, see also text
- Steel/sinter bronze composite
- Steel/PTFE fabric
- Steel/PTFE composite
Recommended fits

Principal dimensions				Angle of tilt	Basic load ratings dynamic	static	Mass	Designation
d	D	B	C	±	C	C_0		
mm				degrees	kN		kg	-
160	230	105	80	8	3800	6400	14,0	**GE 160 TXA-2RS**

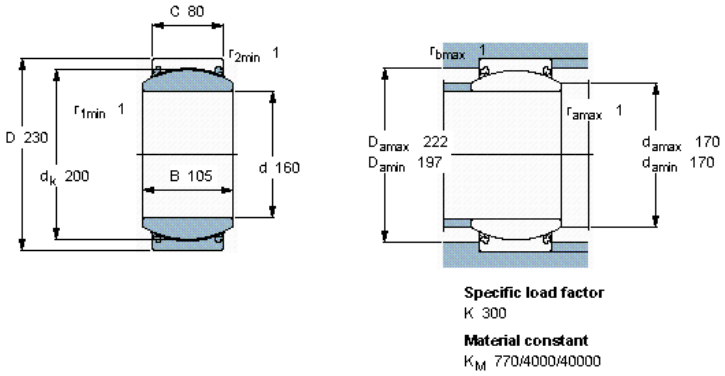

Specific load factor
K 300

Material constant
K_M 770/4000/40000

Figure 33: Pivot Bearing Technical Data

The column assembly attaches to the floor via anchors, which all excess loading is translated into the ground. This can be seen in figure 34 below.

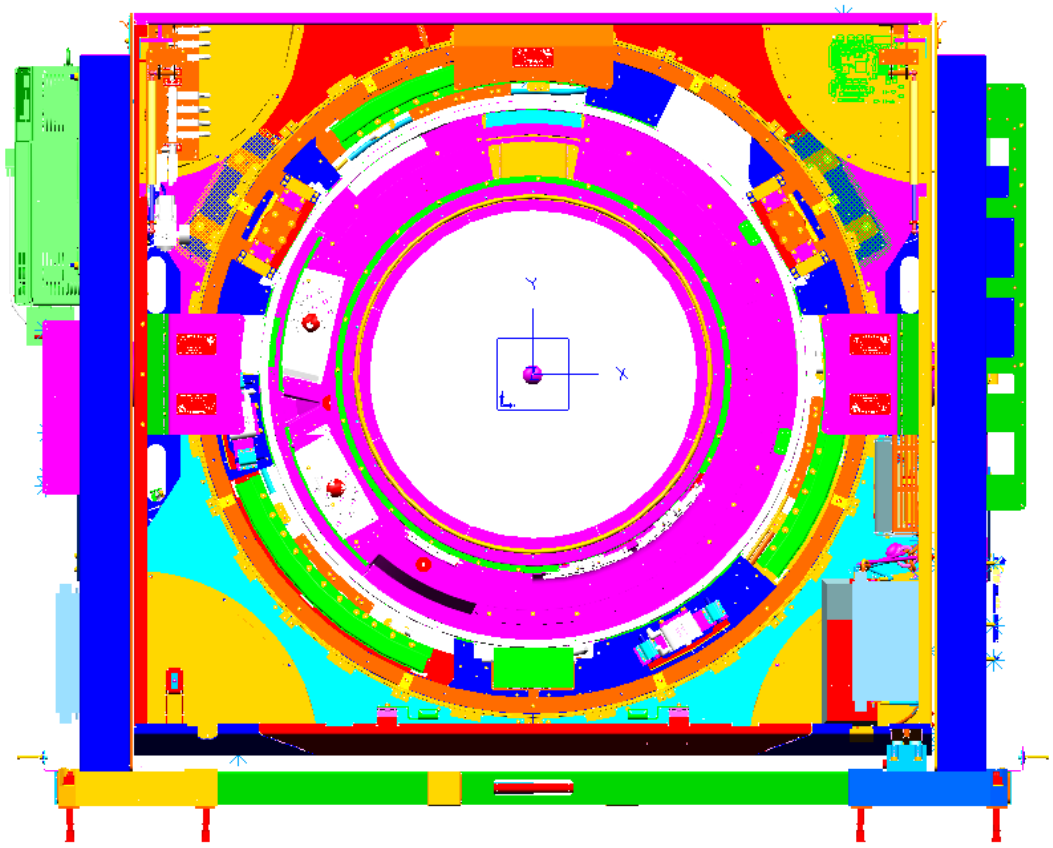

Figure 34: Column Floor Anchors

The tilting portion of the scanner is tilted and held in place from rotational translation by tilt actuators with a designated stiffness. The actuators can be seen in figure 35. These actuators have a particular stiffness which is far less than the rotational stiffness provided so as the speed of the rotating array increases the translation of the tilting stator increases around the pivot bearing. This translation is actually seen as a rocking motion of the tilt box around the pivot point. The completed frame with the actuator can be seen in figure 36 while figure 37 shows the fully assembled gantry.

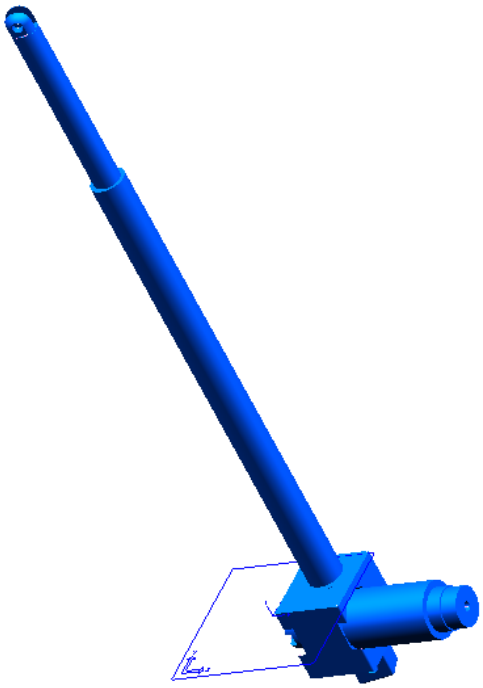

Figure 35: Tilt Actuator

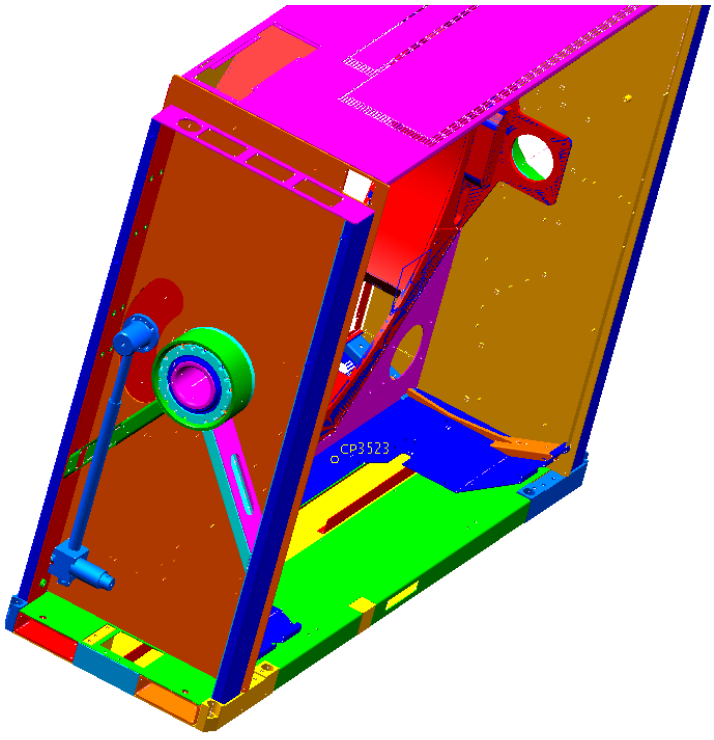

Figure 36: Gantry Assembly with Actuator

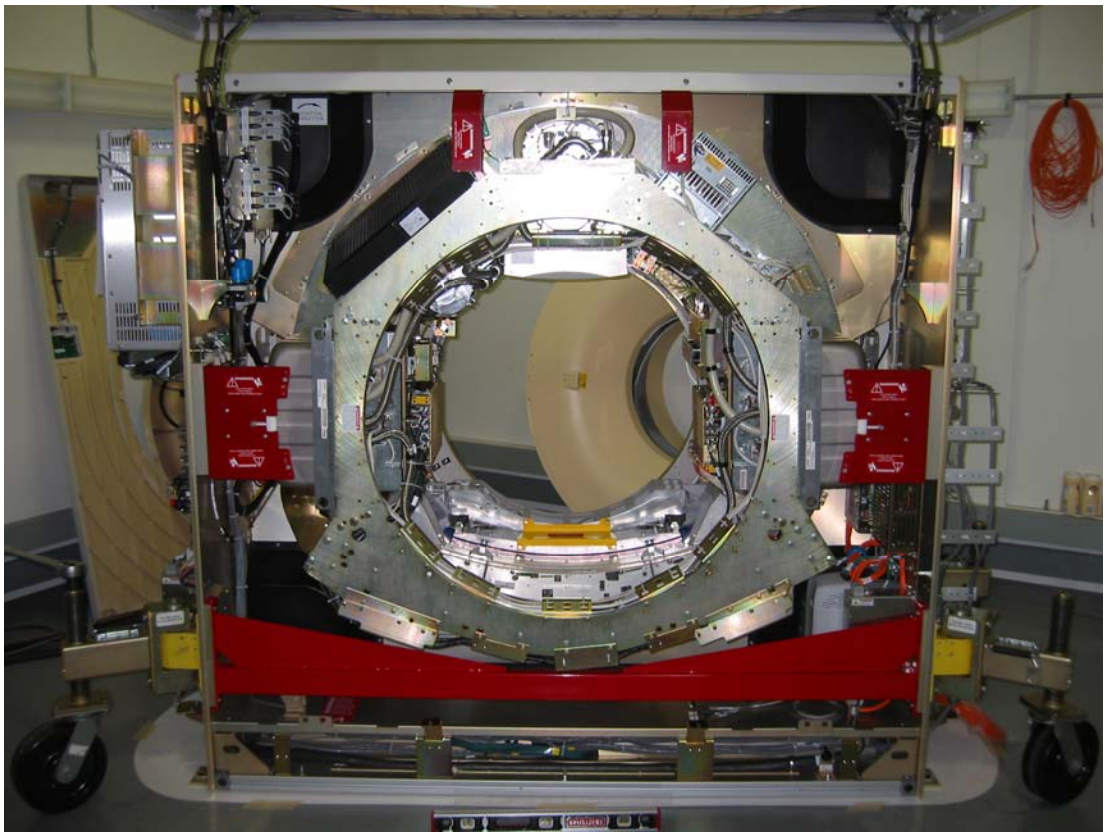

Figure 37: Full Gantry Assembly

Based upon the nature of the CT scanner and the design of the rotor there are two independent types of loading. These independent types of loading produce two types of imbalance. The first type of imbalance is X-Y which will produce displacements in the X-Y plane. This imbalance can be eliminated by using static balancing techniques. Figure 38 demonstrates a static X-Y imbalance.

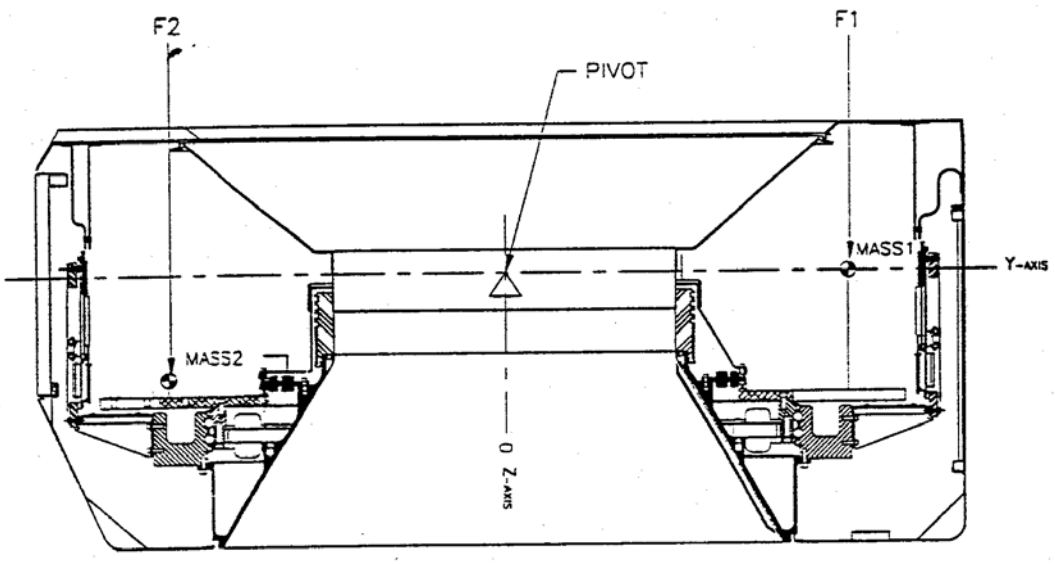

Figure 38: X-Y Balance Illustration

The loaded scan frame can be placed on a theoretical pivot located at the center of rotation. Mass can then be added in the proper amounts and locations such that the rotating portion of the system balances on this pivot. After this balance is obtained it can be stated that the center of mass of the rotating system coincides with the center of rotation.

The second type of imbalance which is produced within the system is Z-plane imbalance. This imbalance effects the displacements, velocities, and accelerations in the z-direction. Figure 39 illustrates the centrifugal acceleration induced moment loading of the scan frame.

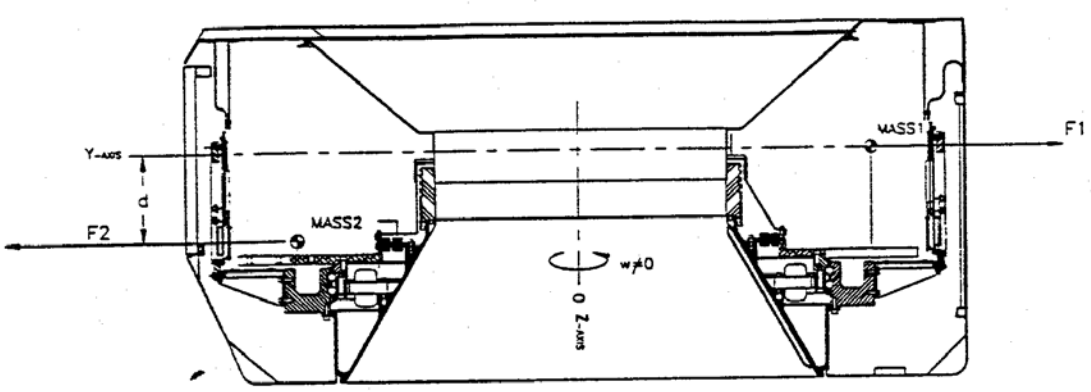

Figure 39: Z-Imbalance Illustration

There is no technique to experimentally static balance this type of loading. Therefore dynamic rotor techniques are typically employed. Similar to the X-Y static balance, a z-displacement is correlated to a moment imbalance. Yet, because of the confined space of the rotor these methods are hard to implement with data acquisition devices. Since there is a known rocking mode that occurs around the pivot point the use of linear transducers are used to find the imbalance of the rotating array.

B. INSTRUMENTATION AND DATA ACQUISITION

CT scanners by nature have limited access for probes, accelerometers, and other measurement devices. The small confinement throughout the CT scanner does not allow for a lot of places for instrumentation around the rotating array. There is also a high necessity for sealed air paths and complete separation of cold and hot sides of these air paths. All these factors add to the complexity of implementing vibrational sensors.

It is minimally invasive to the system to place a transducer on the front side of the tilting frame because of the rocking motion that occurs around the pivot point of the columns. The transducer would correlate the iso-center motion to total rotational translation of the tilt box due to imbalance. The linear transducer used in the balancing process is shown in figure 40.

Figure 40: Linear Transducer

The lead from this transducer was plugged into an analog to digital converter and this response was fed into the oscilloscope for processing. The oscilloscope chosen was an Agilent 35670A-1

The general system schematic that was used for the data collection process is shown below in figure 41:

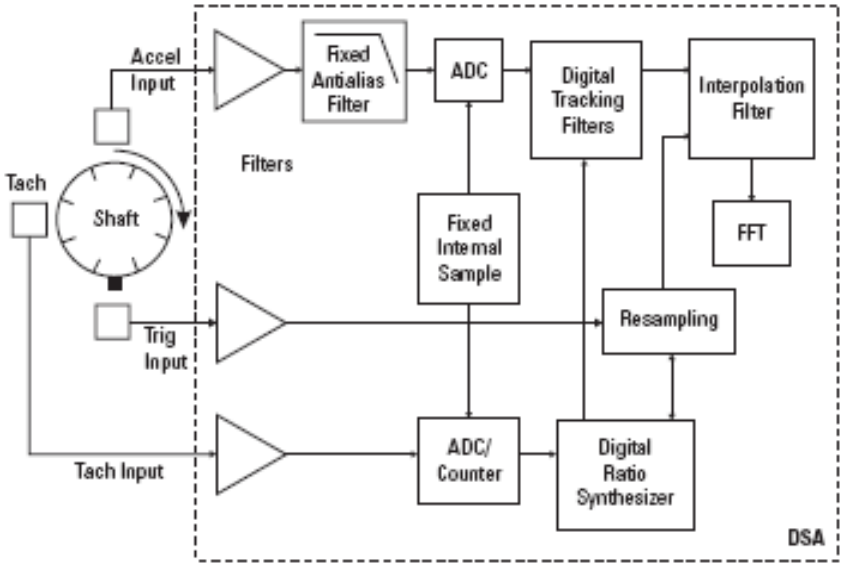

Figure 41: Data Collection Schematic

Based on the schematic above a general outline of the data can be explained. The shaft depiction can be considered the rotating array of the CT scanner. The acceleration input listed above is analyzed through the system software. The system software allows for the user to program the acceleration parameters into the gantry host board which is the brains of the motion system of the scanner. When a given input is sent to the system it is processed as a number based on seconds per revolution. For example, 120 RPM scan is processed as a parameter of 500 ms which means 0.5 second revolutions. This time base can be pulled at a test point on the board to analyze whether or not the system is at the required speed.

The trigger input is captured through the PCB which is inherent to all systems. This rotating PCB is placed on the outer portion of the rotating array and interfaces with a stationary flag assembly. When the rotating PCB goes through the stationary flag assembly a step output is recorded. This tells the gantry at what position is absolute zero. Absolute zero is where the rotor rotates upon initialization of the scanner. This trigger was used in the balancing process so that the rotor angular position was known.

The transducer and trigger data is processed through the oscilloscope listed above and the waveforms are displayed. The transducer data will cycle like a sinusoidal waveform while the trigger data will be displayed as a step function for every revolution. Figure 42 below delineates how a general cycle capture will look per iteration of the balancing procedure.

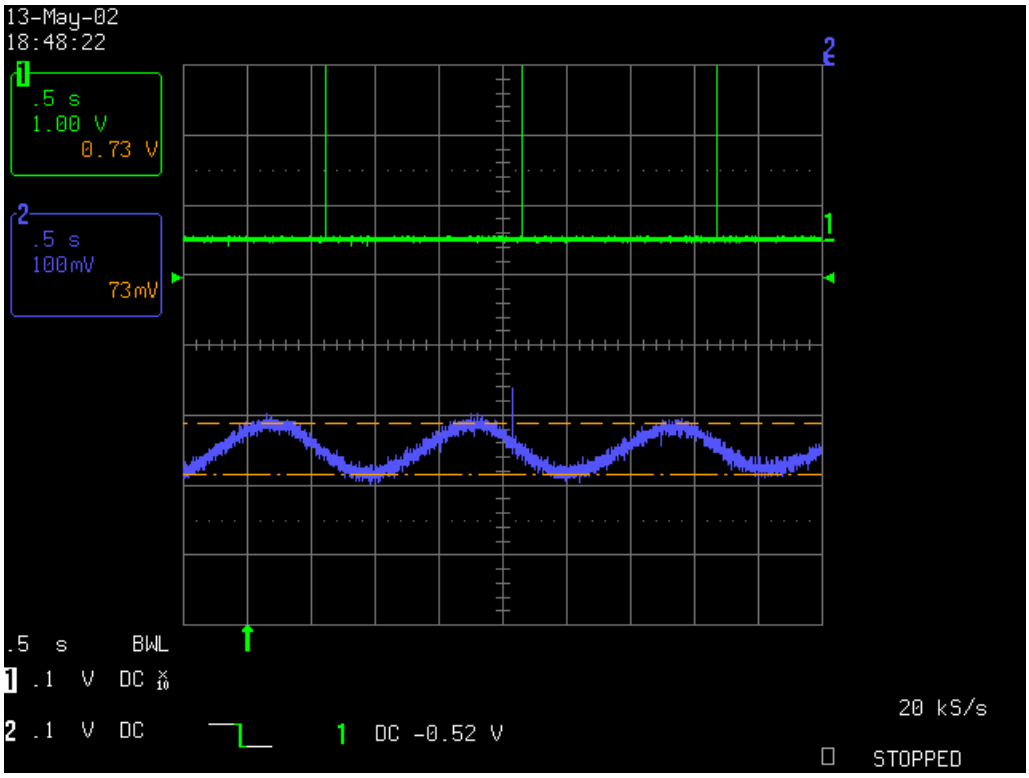

Figure 42: Depiction of Iteration of Balancing

C. METHODOLOGY AND BALANCING PROCEDURE

Balancing a CT scanner is quite unique in its approach because of the corresponding processes that must be taken into consideration based on the fact that the rotating array is loaded in a way of non-uniformity. There are many components that are integral to the CT scanner which are all different weights and have specified coordinates in order to produce the reconstructed image. Because of this matter the balance weight configuration is not performed until all key components have been placed.

There are two distinct processes that have to be completed in order to get the rotating array fully balanced. The first portion is the weight configuration optimization and this is performed by various static balancing techniques while the second portion is based upon dynamic techniques.

a. STATIC BALANCING

The CT scanner rotor is grossly out of balance because the main rotating components are placed in regards to their subsystem requirements. Based upon this fact static balancing is applied first in order to effectively balance the CT scanner. The counterbalance weight configuration is the last thing that is dealt with in the design phase of a new product introduction.

The first step to balancing the rotating array of a CT scanner is to take all of the known CG locations of all the components and make a spreadsheet in order to keep track of where the items are located. Below is an example of how these CG coordinates can be displayed in a spreadsheet. This spreadsheet locates the CG of all the components on the rotor based upon their X, Y, and Z coordinate locations. This chart also calculates the total mass, global CG location of the entire rotor, as well as imbalance of the rotor.

ANTHEM ROTOR ASSEMBLY BALANCE

		CENTER OF GRAVITY				
	Mass	CGx	CGy	CGz	Radius	Angle
Component	[kg]	[mm]	[mm]	[mm]	[mm]	[degrees]
INTERFACE MODULE-FIBER OPTICS	0.64	-0.23	-759.72	-200.02	759.72	269.98
BRACKET-ZERO GATE PCB	0.13	-255.15	807.19	-213.70	846.56	107.54
BRACKET-TUBE CABLE ROUTING	0.15	0.00	819.82	28.82	819.82	90.00
RACE-BEARING	341.27	-0.01	0.27	-409.20	0.27	91.70
ROTOR ASSEMBLY-FRAME	269.95	21.93	22.38	-144.30	31.33	45.58
FASTENER ASSEMBLY-ROTOR	4.62	0.47	32.39	-79.70	32.39	89.18
RING-RESOLVER AND CAPACITIVE MOUNTING	24.95	1.77	-2.20	-294.82	2.82	308.75
BLOCK-X ADJUSTMENT STATIONARY	0.00	187.50	631.52	-3.50	658.77	73.46
LEFT_HAND_Z_ADJUSTMENT_ASSY	0.00	-174.71	668.61	50.61	691.05	104.64
TUBE ADJUSTMENT ASSEMBLY-NEW DESIGN SEPT. 2006	4.47	17.47	658.28	-90.18	658.51	88.48
DMS	94.99	12.99	-470.00	-28.00	470.18	271.58
DUCT-DMS FAB	6.50	-726.03	-277.96	-26.81	777.42	200.95
POWER SLIP RING	30.39	0.56	-3.20	-430.90	3.25	280.00
HVU	80.34	603.00	10.50	-12.00	603.09	1.00
HVU BOOSTER	79.30	-601.10	4.90	25.00	601.12	179.53
XSC	3.53	499.20	401.60	-37.50	640.69	38.82
COOLING UNIT	54.38	-387.00	444.70	-2.00	589.51	131.03
X-RAY TUBE	50.10	4.00	646.00	-0.20	646.01	89.65
FSU	3.60	427.80	377.60	-47.00	570.61	41.43
ANODE DRIVE	13.60	364.50	621.10	-48.00	720.16	59.59
COLLIMATOR	26.08	-3.18	438.85	-26.75	438.86	90.41
DATA RING	22.23	-0.35	-1.30	-359.34	1.35	255.05
CABLES	0.00	1.60	142.90	105.94	142.91	89.36
LH ASTEC POWER SUPPLY	3.90	-410.75	-48.61	-38.98	413.62	186.75
RH ASTEC POWER SUPPLY	3.90	412.65	-69.64	-39.24	418.49	350.42
RPD	3.26	402.10	175.81	-19.49	438.85	23.62
R2D	1.11	-420.99	133.67	-10.78	441.70	162.38
PLATE-TUBE WASHER	0.10	166.00	706.18	-3.50	725.42	76.77
PLATE-TUBE WASHER	0.10	-166.71	706.18	-3.50	725.59	103.28
RING ASSEMBLY-LIM REACTION	32.06	0.00	1.07	-488.70	1.07	90.00
COVER-AXIAL TUBE ACCESS	0.41	-0.06	-667.80	-327.38	667.80	269.99
DUCT-HEAT EXCHANGER	0.91	-491.33	572.33	-246.45	754.30	130.65
BRACKET-HIGH VOLTAGE ROUTING	0.08	-446.99	50.00	-277.65	449.78	173.62
BRACKET-POWER SUPPLY MOUNTING	0.33	-416.86	57.05	-4.50	420.75	172.21
BRACKET-POWER SUPPLY MOUNTING	0.33	-420.56	-154.53	-4.50	448.05	200.18
BRACKET-POWER SUPPLY MOUNTING	0.33	418.73	36.02	4.76	420.28	4.92
BRACKET-ROTOR CABLE RETAINING	0.53	60.79	637.03	222.07	639.92	84.55
BRACKET-ROTOR CABLE RETAINING	0.53	290.87	-579.22	222.07	648.15	296.66
BRACKET-ROTOR CABLE RETAINING	0.53	-416.54	-545.59	222.07	686.42	232.64
BRACKET-ROTOR CABLE RETAINING	0.53	-181.23	-615.04	222.07	641.19	253.58
LASER ASSEMBLY- UPPER LH	0.36	-370.25	231.61	-68.66	436.72	147.97
LASER-ASSEMBLY- UPPER RH	0.34	222.86	436.54	-60.54	490.14	62.96
LASER ASSEMBLY- LOWER RH	0.18	421.95	-209.76	-41.10	471.21	333.57
LASER ASSEMBLY - LOWER LH	0.17	-424.78	-197.84	-41.40	468.59	204.97
BUS-TERMINAL	0.60	310.01	336.84	-288.65	457.79	47.38
COUNTER WEIGHT-LEFT REAR	7.53	-359.93	-650.12	-243.68	743.10	241.03
COUNTER WEIGHT-RIGHT REAR	7.53	359.93	-650.12	-243.68	743.10	298.97
COUNTER WEIGHT-SERVICE PANEL	9.71	0.00	-760.96	-240.90	760.96	270.00
COUNTER WEIGHT - FRONT LEFT -1	5.35	-438.53	-450.91	253.65	628.99	225.80
COUNTER WEIGHT - FRONT LEFT -2	0.00	-438.53	-450.91	250.48	628.99	225.80
COUNTER WEIGHT - FRONT LEFT -3	0.00	-438.53	-450.91	248.89	628.99	225.80
COUNTER WEIGHT - FRONT LEFT -4	0.00	-438.53	-450.91	229.84	628.99	225.80
COUNTER WEIGHT - FRONT MIDDLE -1	2.48	-0.08	-584.88	255.24	584.88	269.99
COUNTER WEIGHT - FRONT MIDDLE -2	2.48	-0.08	-584.88	245.71	584.88	269.99
COUNTER WEIGHT - FRONT MIDDLE -3	2.48	-0.06	-584.86	234.60	584.86	269.99
COUNTER WEIGHT - FRONT MIDDLE -4	3.31	-0.06	-584.86	226.25	584.86	269.99
COUNTER WEIGHT - FRONT MIDDLE -5	0.00	-0.06	-584.86	209.20	584.86	269.99
COUNTER WEIGHT - FRONT RIGHT -1	4.21	449.78	-445.64	256.83	633.16	315.26
COUNTER WEIGHT - FRONT RIGHT -2	4.21	449.78	-445.64	248.89	633.16	315.26
COUNTER WEIGHT - FRONT RIGHT -3	4.21	449.78	-445.64	239.36	633.16	315.26
COUNTER WEIGHT - FRONT RIGHT -4	4.21	449.78	-445.64	226.66	633.16	315.27
COUNTER WEIGHT - FRONT RIGHT -5	5.63	449.78	-445.64	215.55	633.16	315.27
COUNTER WEIGHT - REAR FAR LEFT -1	1.91	-485.00	-585.40	-230.95	760.21	230.36
COUNTER WEIGHT - REAR FAR LEFT -2	1.91	-485.00	-585.40	-218.25	760.21	230.36
COUNTER WEIGHT - REAR FAR LEFT -3	1.91	-485.00	-585.40	-205.55	760.21	230.36
COUNTER WEIGHT - REAR FAR LEFT -4	1.91	-485.00	-585.40	-192.85	760.21	230.36
COUNTER WEIGHT - REAR MIDDLE LEFT -1	1.91	-355.00	-662.78	-230.95	751.86	241.83
COUNTER WEIGHT - REAR MIDDLE LEFT -2	0.00	-355.00	-662.78	-218.25	751.86	241.83
COUNTER WEIGHT - REAR MIDDLE LEFT -3	0.00	-355.00	-662.78	-205.55	751.86	241.83
COUNTER WEIGHT - REAR MIDDLE LEFT -4	0.00	-355.00	-662.78	-192.85	751.86	241.83
COUNTER WEIGHT - REAR NEAR LEFT -1	0.00	-225.00	-729.67	-230.95	763.57	252.86
COUNTER WEIGHT - REAR NEAR LEFT -2	0.00	-225.00	-729.67	-218.25	763.57	252.86
COUNTER WEIGHT - REAR NEAR LEFT -3	0.00	-225.00	-729.67	-205.55	763.57	252.86
COUNTER WEIGHT - REAR NEAR LEFT -4	0.00	-225.00	-729.67	-192.85	763.57	252.86
COUNTER WEIGHT - REAR NEAR RIGHT -1	0.00	225.00	-729.67	-230.95	763.57	287.14
COUNTER WEIGHT - REAR NEAR RIGHT -2	0.00	225.00	-729.67	-218.25	763.57	287.14
COUNTER WEIGHT - REAR NEAR RIGHT -3	0.00	225.00	-729.67	-205.55	763.57	287.14
COUNTER WEIGHT - REAR NEAR RIGHT -4	0.00	225.00	-729.67	-192.85	763.57	287.14
COUNTER WEIGHT - REAR MIDDLE RIGHT -1	0.00	355.00	-662.78	-230.95	751.87	298.17
COUNTER WEIGHT - REAR MIDDLE RIGHT -2	0.00	355.00	-662.78	-218.25	751.87	298.17
COUNTER WEIGHT - REAR MIDDLE RIGHT -3	0.00	355.00	-662.78	-205.55	751.87	298.17
COUNTER WEIGHT - REAR MIDDLE RIGHT -4	0.00	355.00	-662.78	-218.25	751.87	298.17
COUNTER WEIGHT - REAR FAR RIGHT -1	0.00	485.00	-585.40	-230.95	760.21	309.64
COUNTER WEIGHT - REAR FAR RIGHT -2	0.00	485.00	-585.40	-218.25	760.21	309.64
COUNTER WEIGHT - REAR FAR RIGHT -3	0.00	485.00	-585.40	-205.55	760.21	309.64
COUNTER WEIGHT - REAR FAR RIGHT -4	0.00	485.00	-585.40	-192.85	760.21	309.64
PERFECT WEIGHT 1	4.45	713.89	-344.17	5.08	792.53	334.26
PERFECT WEIGHT 2	3.00	727.35	-335.74	50.00	801.10	335.22
PERFECT WEIGHT 3	2.00	265.78	522.59	104.00	586.29	63.04

	Mass	CGx	CGy	CGz	Radius	Angle
Rotating Array Totals	[kg]	[mm]	[mm]	[mm]	[mm]	[degrees]
	1244.13	0.11	0.08	-181.81	0.140	36.00

Rotational Speed	220	RPM		
Total X-Y Imbalance	X	0.11	[mm]	
	Y	0.08	[mm]	
	FORCE	92.70	[N]	
Total Couple Imbalance	Txz	52.49	[N-m]	
	Tyz	27.00	[N-m]	
	Tz	59.03	[N-m]	
	ANGLE	27.22	[degrees]	
Torque on Tilt Pivots	Tilt Axis	-2216.66	[N-m]	

IMBALANCE	
0.01	N-m
0.01	lbf-ft

Table 7: CG Location Chart

Table 7 above is used in the dynamic balancing program. The program is written in Matlab and is used to calculate the counterbalance weights and locations. This data can be used to optimize the weight configuration and imbalance corrections in the design phase of the CT scanner. The component CG coordinates and their according weights are inserted into a text file and imported into Matlab. The results of this M-file show the magnitude and the corresponding location of the counterbalance weights needed to lower the imbalance of the rotor. The program is not used for the final balancing of the rotor; it is merely a tool that can be used in a manufacturing setting in order to get a rough static balance of the rotor. This tool assures that the rotor is able to be rotated by hand without having any safety concerns.

b. DYNAMIC RIGID ROTOR BALANCING

Dynamic rotor techniques are implemented to extrapolate the imbalance frequencies of the rotor. These techniques have to be employed because there are many frequencies throughout the system. Using the given equipment and Matlab a Fourier series decomposition is performed on the test data. The Fourier series decomposition provides the 2 Hz fundamental frequency and this data is used to fine tune the balance of the system.

The first step in this process is placing the linear transducer in the designated place on the frame. This placement is at the bottom of the tilt frame 2” up from the column assembly. The transducer placement can be seen below in figure 43.

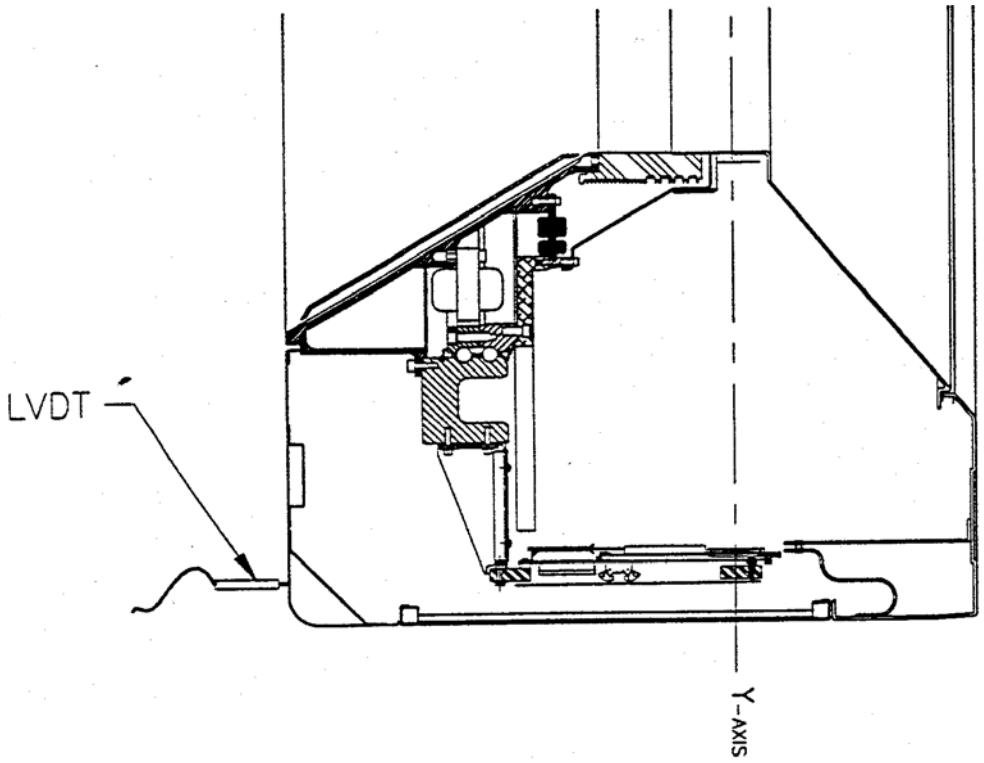

Figure 43: Transducer Placement

The displacement plot from the oscilloscope is shown below, in figure 44, to give an example of the initial trial run.

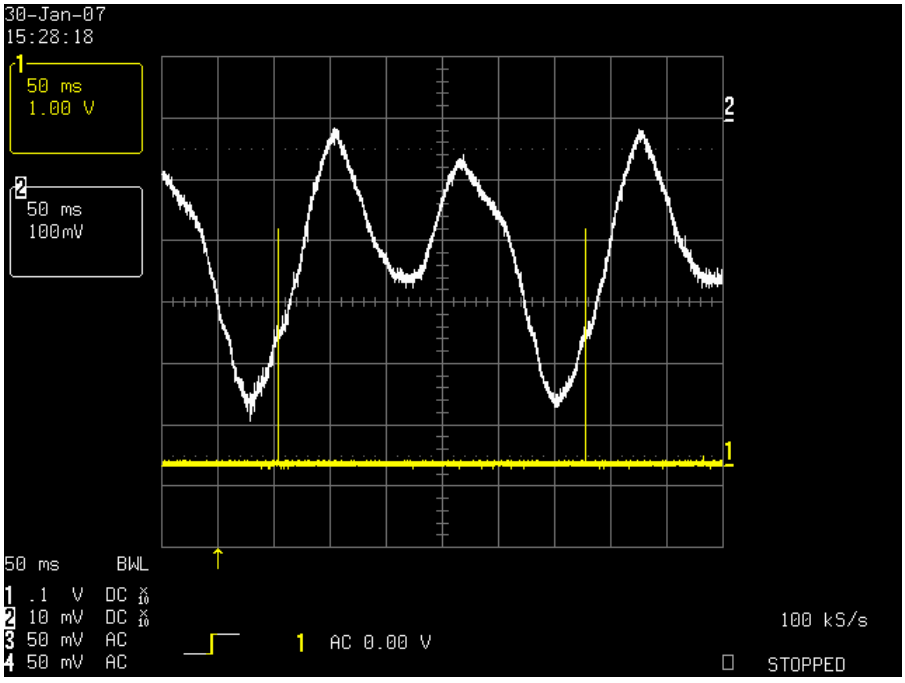

Figure 44: Trial Run of Displacement Plot

The figure above has two different plots. The first plot (yellow) indicates one full revolution of the rotor while the second plot (white) is the response of the tilt frame. This data from the oscilloscope is taken and imported into Matlab. Once the data is imported into Matlab a Fourier series decomposition is used to extract the 2 Hz fundamental frequency. The 2 Hz fundamental frequency is then used to balance the CT scanner rotor. Figure 45 below depicts a Fourier series decomposition of the 2 Hz fundamental frequency.

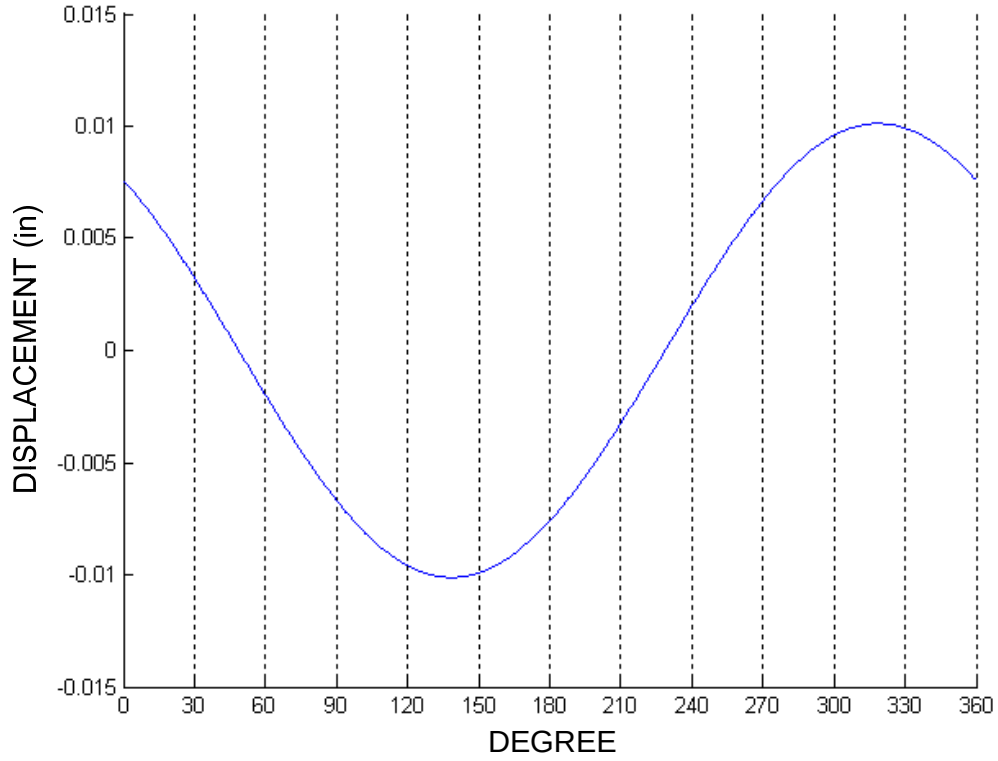

Figure 45: Vibration Signal at Fundamental Frequency of 2 Hz

The 2 Hz frequency is used because imbalance happens once per revolution. The balancing speed was 120 RPM (2 Hz) which is why the Fourier series decomposition pulls this designated frequency. Once the 2 Hz fundamental frequency was observed the magnitude of the imbalance had to be decided. In order to determine the magnitude of the

imbalance, a relationship between the imbalance and the imbalance deflection must be established. The relationship is derived experimentally by imposing a known moment change of imbalance and measuring the deflection. Figure 46 below shows a generic rotor layout of the CT scanner.

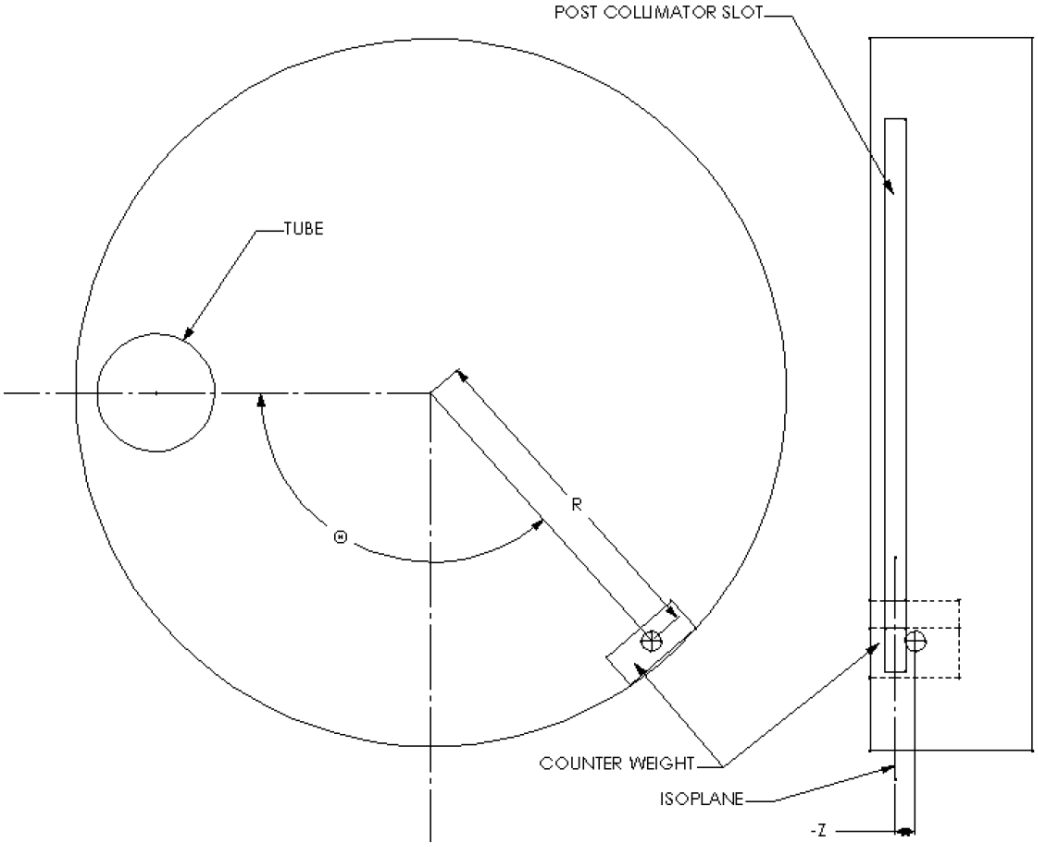

Figure 46: Rotor Schematic

Common		Configuration 1		Configuration 2		Configuration 3	
Weight (lb)	R (in)	Φ (degree)	Z (in)	Φ (degree)	Z (in)	Φ (degree)	Z (in)
2.20	33.75	248.99	0.50	248.99	-9.69	248.99	-9.69
3.30	33.50	231.19	0.75	231.19	-9.75	231.19	-9.75
4.00	33.44	194.01	1.25	194.01	1.25	194.01	-5.81
4.40	33.22	130.51	1.00	130.51	1.00	130.51	-3.75

Table 8: Counterweight Configurations

The responses of the three weight configurations above in table 8 are shown below in figure 47.

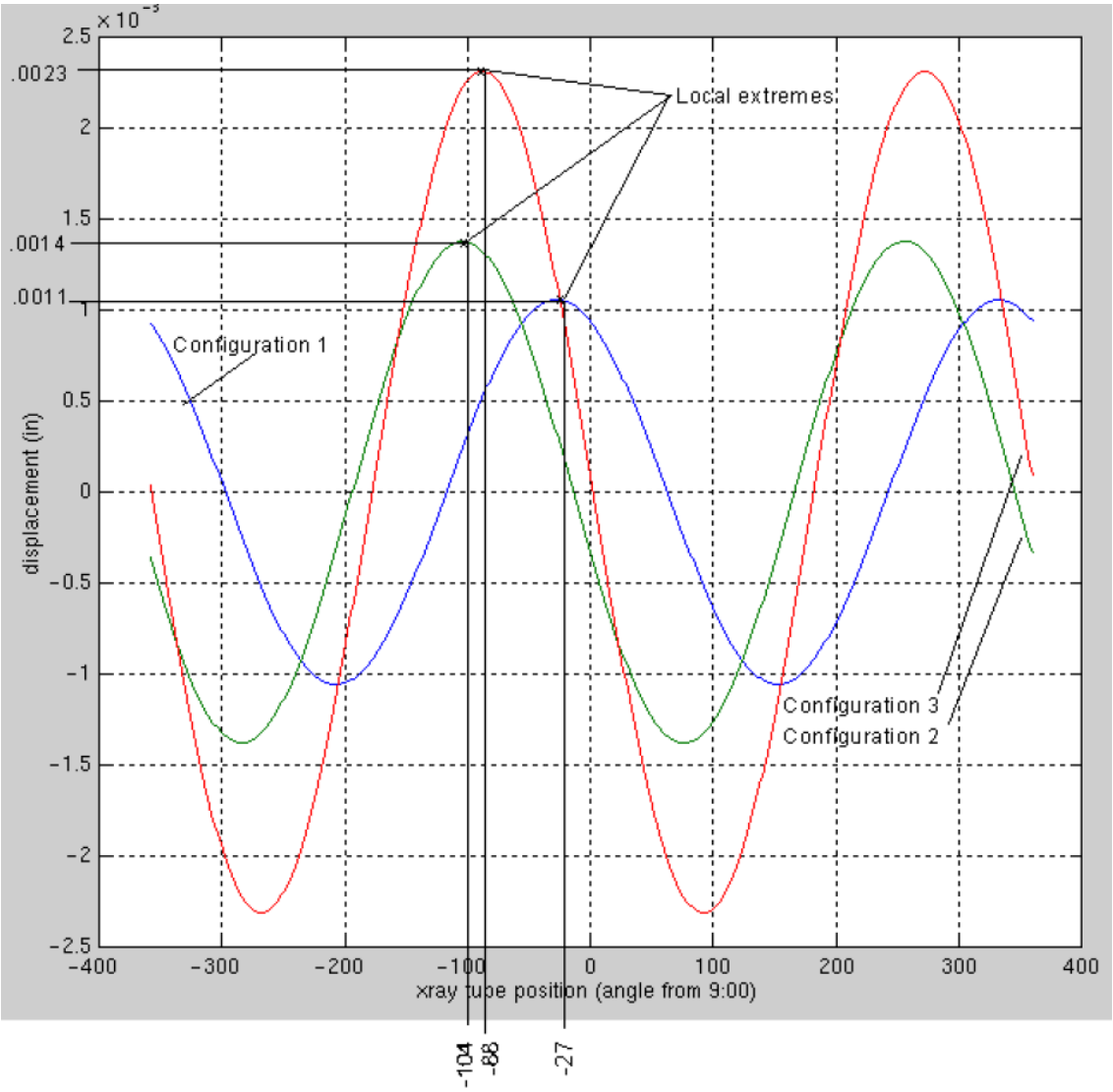

Figure 47: Z-Axis Displacement of Trial Weights

These extreme displacements of figure 47 can be plotted as vectors shown in figure 48 below.

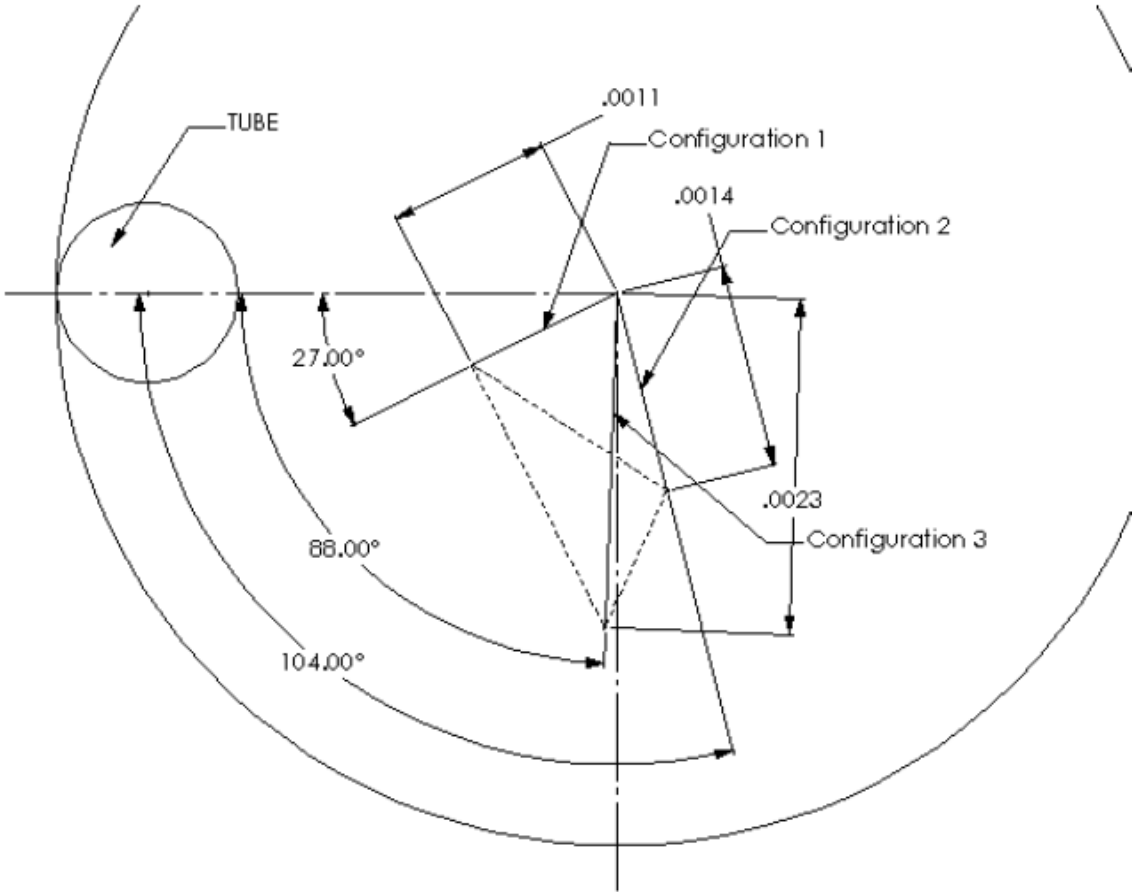

Figure 48: Vector Representation of Extreme Displacement Values

The moment load change between configurations can be estimate by:

$$\Delta T_x = \sum Mr\omega^2 \delta Z_i \sin\Theta \tag{5.1}$$

$$\Delta T_y = \sum Mr\omega^2 \delta Z_i \cos\Theta \tag{5.2}$$

with the total torque change:

$$\Delta T = \sqrt{\Delta T_x{}^2 + \Delta T_y{}^2} \tag{5.3}$$

applied in direction:

$$\Theta_{\Delta T} = \tan^{-1}\frac{\Delta T_x}{\Delta T_y} \tag{5.4}$$

Using equations 5.3 and 5.4 a graphical representation of the vectors can be shown. These vectors are shown below in figure 49. The dashed lines can be used to determine a correlation between z-imbalance torque and extreme z-axis displacement.

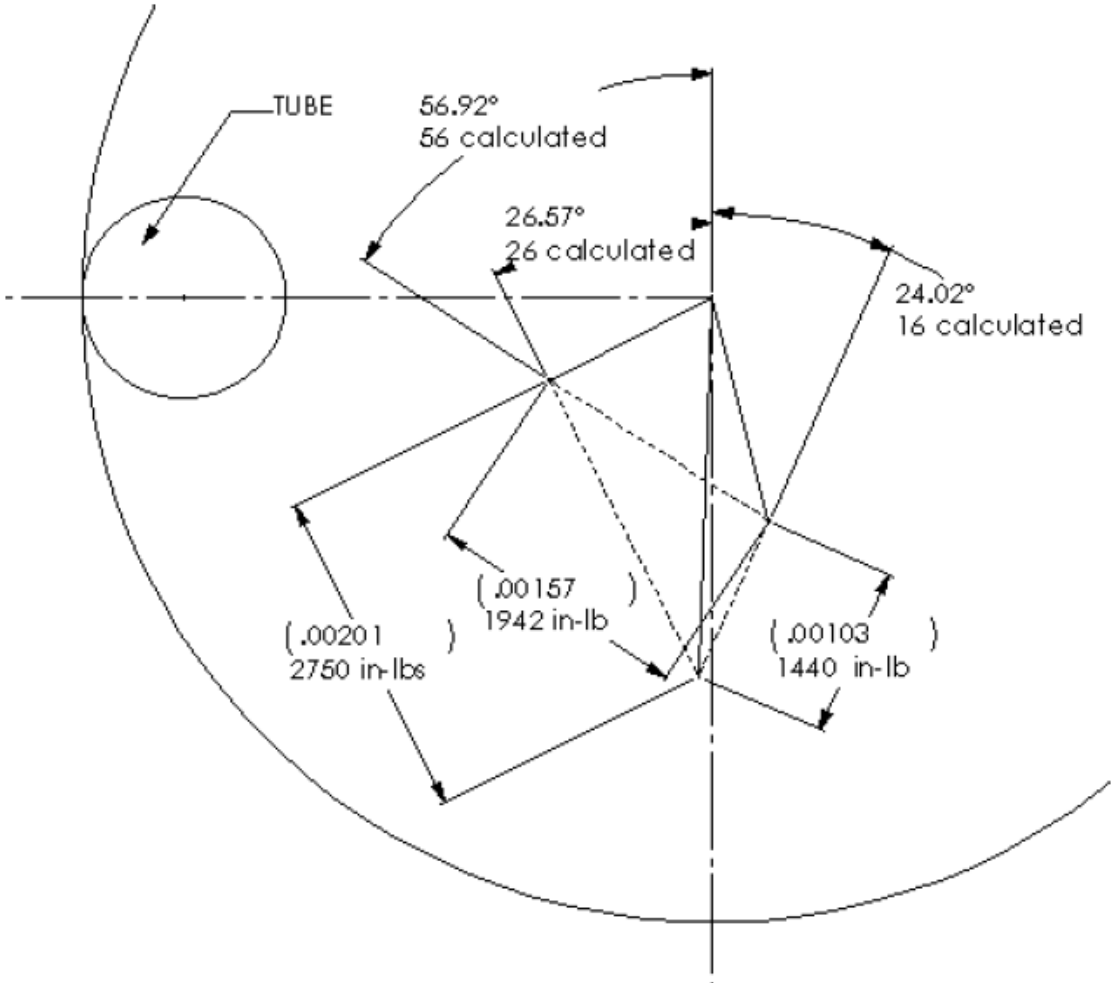

Figure 49: Imbalance / Displacement Correlation Graphical

Configuration		Θ (degree)		Change in Torque		Correlation
From	To	$\Theta_{Calculated}$	$\Theta_{Graphical}$	Calculated (in-lb)	Graphical (in-lb)	K (in-lb/in)
1	2	56	57	1942	0.00157	1 236 900
1	3	26	27	2750	0.00201	1 368 200
2	3	16	24	1440	0.00103	1 398 900

Table 9: Imbalance / Displacement Correlation

Figure 49 and table 9 show the correlation factors of imbalance to displacement. This iterative process was concluded after three configurations. The trial runs for this procedure resulted in three different weight configurations.

D. RESULTS

Based upon the findings above the rotating array imbalance was reduced by about a factor of eight. This was accomplished in three iterations of trials with weight additions each time. The three Fourier series decomposition plots are shown in figure 50 – 52:

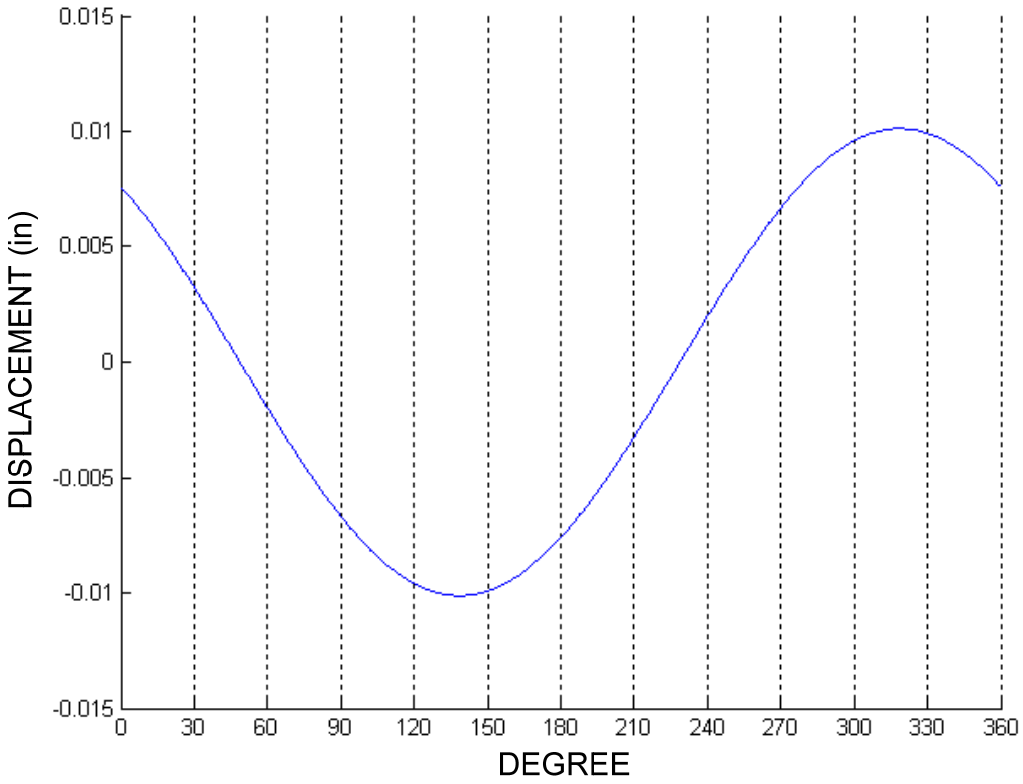

Figure 50: Fourier Series Decomposition Trial 1

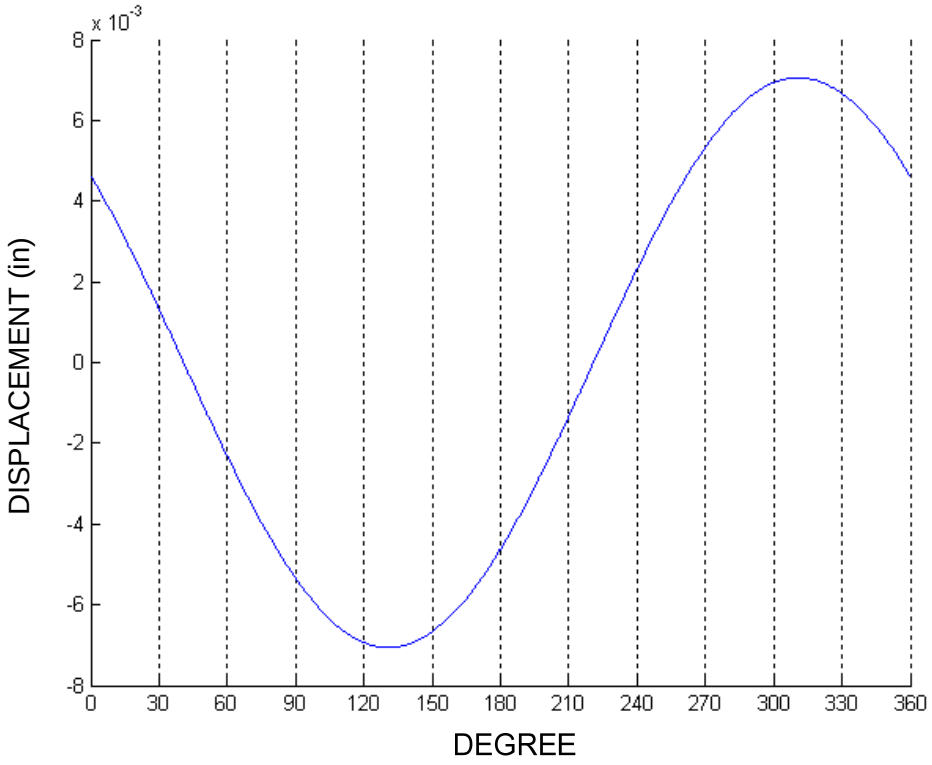

Figure 51: Fourier Series Decomposition Trial 2

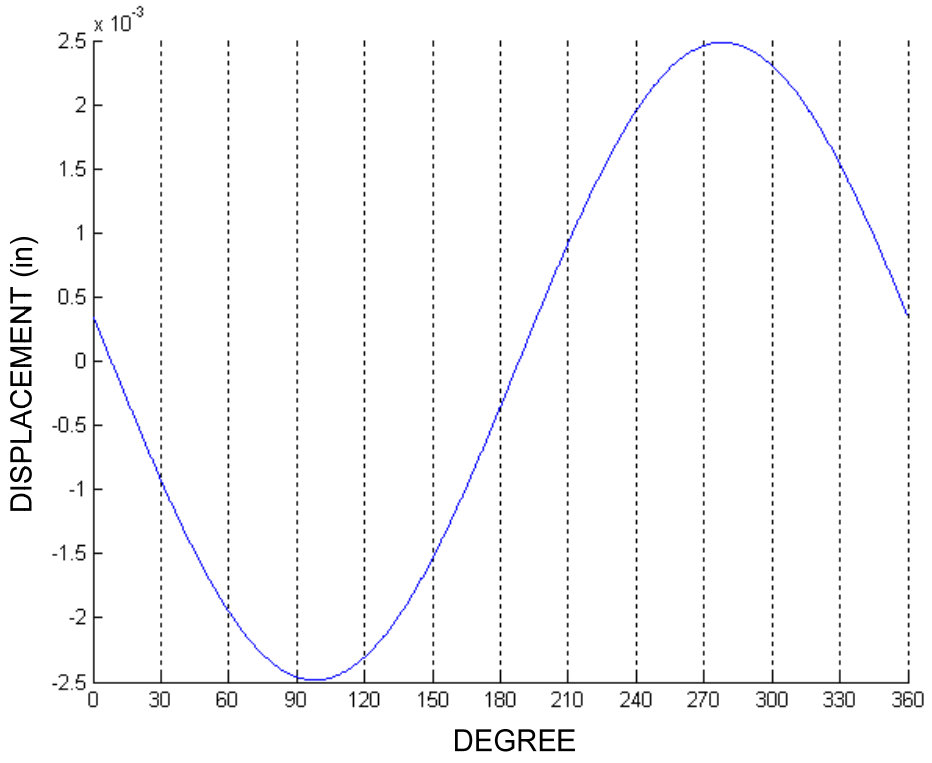

Figure 52: Fourier Series Decomposition Trial 3

The corresponding weights that were added to the system are shown below in Table 10. The initial rotor response and final rotor response are shown below in figure 53.

Weight (lb)	R (in)	Φ (degree)	Z (in)
3.20	33.25	115	2.88
2.90	33.25	297	-12.00
1.50	34.03	264	3.69

Table 10: Final Weight Configurations

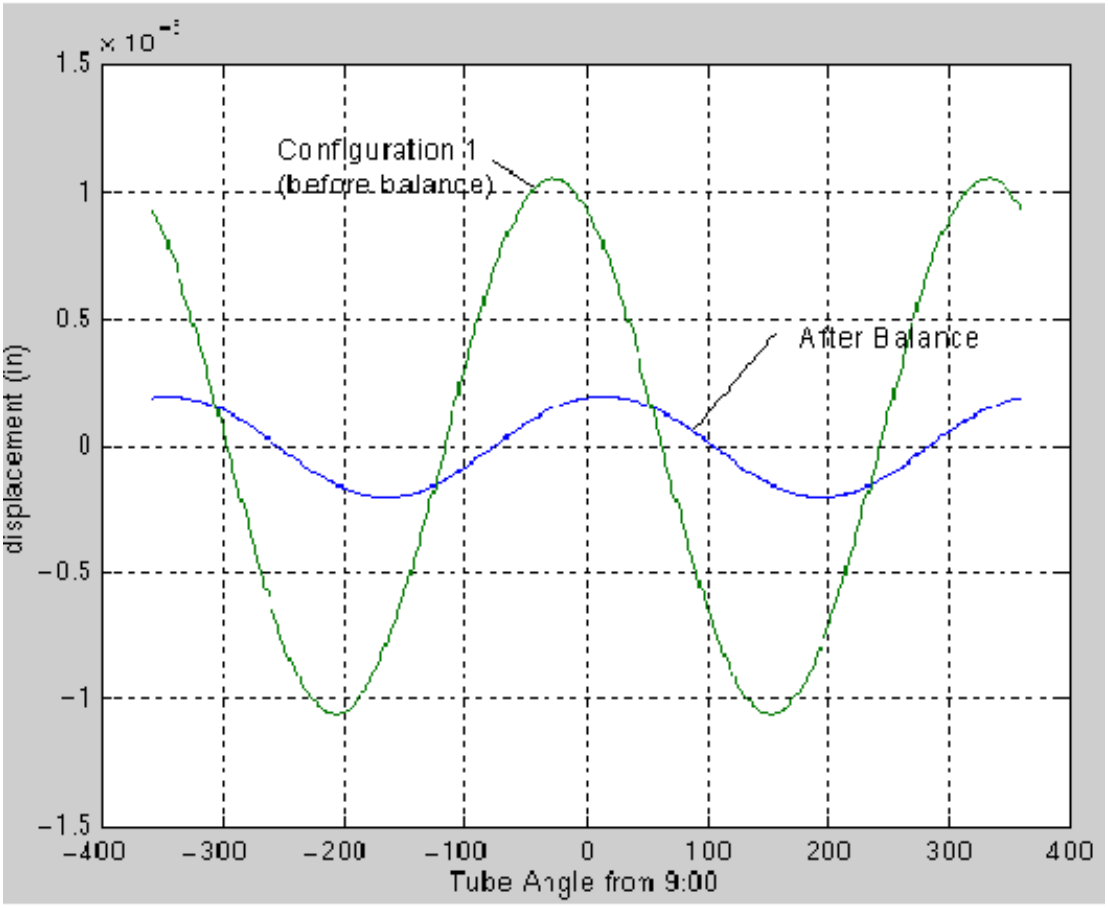

Figure 53: Final Imbalance Response

The LVDT results can be compared to a mechanical indicator reading. The mechanical indicator reading was reduced from 0.0085" to 0.0014" at the optimum balancing speed. Based upon these findings it can be assumed that the rotor imbalance

and the methods used are satisfactory in an industrial setting to effectively balance a CT scanner rotating array.

CHAPTER VI

CONCLUSIONS

A. DISCUSSION

The proposed topic of this thesis was the development of an effective balancing procedure for CT scanners. Rigid and flexible rotor balancing techniques were discussed in order to establish this procedure. The flexible rotor balancing technique of influence coefficient method was used to balance an experimental rotor test rig. The balancing knowledge gained from the experimental rotor test rig was applied to the CT scanner rotor. Aspects of the influence coefficient method were employed in the rigid rotor balancing techniques used to balance the CT scanner rotor. A known imbalance was put into the rotor assembly of the CT scanner and the imbalance was correlated to the transducer reading in order to calculate the counter balance weights. This is the same fundamental approach that the flexible rotor balancing technique of influence coefficient method uses in order to calculate the counterbalance weights. This developed procedure uses main stream rigid rotor balancing techniques with rudimentary aspects of influence coefficient method to balancing the CT scanner rotor in a manufacturing setting.

The implementation of the CT scanner rotor balancing method has been proven to work in a manufacturing environment. This procedure will ultimately work on any CT scanner as long as following three conditions are satisfied:

- The CT scanner rotor operates more than 20% below its first natural frequency
- The stiffness of the tilting portion of the CT tilting frame is far more than the translational stiffness in the actuators.
- The rotor is an overhung and all loading is held primarily to the rotating array.

The simulated data and balancing method for CT scanner has been presented throughout this thesis. All pertinent information and the evaluation of the effectiveness of the balancing procedure have been documented. The magnitude of the imbalance of the CT scanner rotor was reduced by a factor of eight. The analysis and techniques have been designed from the basics of rotordynamics with a more business oriented approach.

The developed approach has significant impact in the CT manufacturing field based on how the process works. The procedure provides a low cost, safe, reliable, and repeatable way to balance a CT scanner rotor.

B. RECOMENDATIONS FOR FUTURE WORK

There is one exclusive aspect that can be taken into consideration with this process which is the endless technical advancements in the Computed Tomography field which ultimately drives every product line. There is a continuous pursuit for faster and clearer images. The only way this can be completed is through more power to the X-ray tube and a faster rotating array. The tube portion of this brings the clearer images while the faster rotational speeds allow the hospitals to examine more patients in a shorter

amount of time. There is also a high demand for wider imaging planes which in turn makes the DMS deeper.

All of these demands whether they are market or consumer driven make the rotating array heavier. Heavier components cause the rotating array to have a higher moment of inertia and with the heavier loading of the rotor the faster it will spin. As the rotor spins faster the imbalance goes higher. With the more powerful X-ray component there is also a higher need to move the focal spot of the system which can cause a 185 lb CG to shift in the Z-direction up to 20 mm. This alone causes an extreme imbalance shift in the rotating array leading to the desired active balancing device that would be inherent to all systems.

This active balancing device would have an integrated load cell to the bearing of the rotating system. This load cell would capture data continuously in order to find the imbalance of the system. The load cell response would be used to calculate the imbalance of the rotor at any speed. This data would then correlate to a movement of predetermined balance weights on the rotor which would correct the imbalance of the system. The process could be done at any given time if the system was initialized. This process would be state of the art for the CT scanner field. It would be a breakthrough that has been a common plight for CT manufacturers the pursuit to make faster and clearer images.

REFERENCES

J. G. Baker, Methods of rotor-unbalance determination, Trans. American Society of Mechanical Engineers, J. Applied Mechanics **61** (1939), A1 – A6.

R. E. D. Bishop, The vibration of rotating shafts, J. Mechanical Engineering Science **1**(1) (1959), 50-65.

R. E. D. Bishop and G. M. L Gladwell, The vibration and balancing of an unbalanced flexible rotor, J. Mechanical Engineering Science **1**(1) (1959), 66-77.

M. P. Blake, Using phase measuring to balance rotors in place, Hydrocarbon Processing (1967), 127-132.

M. S. Darlow, A unified approach to the mass balancing of rotating flexible shafts, Ph.D. thesis, University of Florida, June 1980.

M. S. Darlow, Balancing of high-speed machinery: Theory, methods and experimental results, Mechanical Systems and Signal Processing **1**(1) (1987), 105-134.

W. C. Foiles, Advanced techniques on multi-plane balancing of high speed flexible rotor-bearing systems, Master's thesis, School of Engineering and Applied Science, University of Virginia, Charlottesville, Virginia, 1982.

E. J. Gunter, L. E. Barrett and P. E. Allaire, Balancing of multi-mass flexible rotors: Part I theory and part II experimental results, in: Proc. 5th Turbomachinery Symposium, College Station, Texas, October 1976, Texas A&M University.

R. P. Kroon, Balancing of Rotating Apparatus – II, Journal of Applied Mechanics, March 1944, A47 – A50.

C. Jackson, Back to the Fundamentals – Understanding Rotor Resonance, Sound and Vibration (1993), 8 – 13.

W. C. Foiles, P.E. Allaire and E.J Gunter, Review: Rotor balancing, Shock and Vibration **5** (1998) 325-336.

G. A. Hassan, New Approach for Computer-Aided Static and Dynamic Balancing of Rigid Rotors, Journal of Sound and Vibration **179** (1995), 749-761.

F. F. Ehrich, *Handbook of* Rotordynamics, Mcgraw-Hill, 1992.

J. M. Vance, Rotordynamics of turbomachinery, John Wiley & Sons, 1988.

D. Norfield, Practical Balancing of Rotating Machinery, Elsevier, 2006.

D. E. Bently, Fundamentals of Rotating Machinery Diagnostics, Bently Pressurized Bearing Company, 2002.

N. F. Rieger, Balancing of rigid and flexible rotors, The Shock and Vibration Information Center, Naval Research Laboratory, Washington, DC, 1986.

J. W. Rogers, Notes on balancing rotating masses, Mech. World **71**(1832) (1921 or 22), 106 – 107.

J. M. Tessarik, Flexible rotor balancing by exact point-speed influence coefficient method, MTI-70tr59, NASA, Lewis Research Center Cleveland, Ohio, October 1970.

E. L. Thearle, Dynamic balancing of rotating machinery in the field, Trans. American Society of Mechanical Engineers, J. Applied Mechanics **56**(1934), 745 – 753.

L. Shi, A Modified Balancing Method for Flexible Rotors Based on Multi-sensor Fusion, Journal of Applied Sciences, **5**(2005), 465 – 469.

A. Foppl, Das problem der lavalschen turbinenwelle, Der Civilingenieur **4**(1895), 335 – 342.

H. H. Jeffcott, The lateral vibration of loaded shafts in the neighborhood of a whirling speed – the effect of want of balance, Philosophical Magazine **37**(1919), 304 – 314.

B. Xu and L. Qu, A new practical modal method for rotor balancing, Proceedings of the I MECH E Part C Journal of Mechanical Engineering Science, **215**(2001), 179 – 189.

M. L. Adams, Rotating Machinery Vibrations From Analysis to Troubleshooting, CRC Press, 2000.

APPENDICES

A. MATLAB CODE CG DYNAMIC BALANCE

```
clear

%momwt=1;
%mmin=600;
load AR.txt;
m=AR(:,1);                          %kg
X=AR(:,2:4);                        %mm

x=X(:,1);                           %mm
y=X(:,2);                           %mm
z=X(:,3);                           %mm

Mx=sum(m.*x);
My=sum(m.*y);

Tsx=-sum(m.*y)                      %kg-mm
Tsy=sum(m.*x)                       %kg-mm
%Tsz=sum(m.*z);                     %kg-mm
%Tw=[0 0];

w=220*2*pi/60;                      %rad/s
g=9800;                             %mm/s^2

%TTs=m.*(x.^2+y.^2);
%TTd=w^2/g*sqrt(x.*x+y.*y).*z.*m;
Tdx=-sum((m.*w^2).*y.*z./g)         %kg-mm
Tdy=sum((m.*w^2).*x.*z./g)          %kg-mm
%T=[Tsx;Tsy;Tdx;Tdy];
%T=[Tsx;Tsy];

%ww=0;
%k=0;
%s=m;
%hlow=0;

%Constants

R=590;  %R=750;                     %mm
zmax=260;                           %mm
zmin=-250;                          %mm
%FINDING X-Y BALANCE LOCATION

thmin=atan(-Tsx/Tsy);
%thmin=atan(-My/Mx)                 %CHANGES!!!
```

```
M=sum(m);                              %kg
Rcg=sqrt(Tsx^2+Tsy^2)/M;                    %mm

mbmin=M*Rcg/R;                         %kg
xbmin=[cos(thmin) sin(thmin)]*R;            %mm

mt=[m;mbmin];
xt=[x;xbmin(:,1)];
yt=[y;xbmin(:,2)];

%FINDING THE Z-LOCATION OF THE COUNTERWEIGHT

Tzmin=inf;

for z1=zmax:-.05:zmin;

zt=[z;z1];
Tdx=-sum((mt.*w^2).*yt.*zt./g);
Tdy=sum((mt.*w^2).*xt.*zt./g);
Tz=sqrt(Tdx^2+Tdy^2);

if ((Tz<Tzmin));

        zbmin=z1;
        %Txmin=Tdx;
        %Tymin=Tdy;
        Tzmin=Tz;
   %Tw=[Tw; [zbmin' Tz]];
   zth=atan(Tdy/Tdx)- pi/2;                 %CHANGES!!
   Mz=Tz./w^2/R/(zmax-zmin)*g;

end;
end;

%FINDING THE Z-COUNTERBALANCE

xt=[xt;cos(zth)*R;-cos(zth)*R];
yt=[yt;sin(zth)*R;-sin(zth)*R];
zt=[z;zbmin;zmax;zmin];
mt=[mt;Mz;Mz];

%CHECKING RESULTS

Tdx=-sum((mt.*w^2).*yt.*zt./g)              %N-m
Tdy=sum((mt.*w^2).*xt.*zt./g)               %N-m
```

```
Tz=sqrt(Tdx^2+Tdy^2)
Tsx=-sum(mt.*yt)                %N-m
Tsy=sum(mt.*xt)                 %N-m

balance=[mbmin xbmin zbmin;Mz cos(zth)*R sin(zth)*R zmax;Mz -cos(zth)*R -
sin(zth)*R zmin]
```

B. MATLAB FOURIER SERIES DECOMPOSITION CODE

```
function [amplitudes] = fourier(data, order)

   close all;

   [M2,N2]=size(data);

   if M2>1000

   samples=1000;
   [M1,N1]=size(data);
   index1=M1/samples;
   average=mean(data);
   data=data-average;
   X=[1:M1];
   Xnew=[1:samples];
   X1=index1*Xnew;
   Y1=interp1(X,data,X1);
   data=Y1';
end

   % Get length of data vector or number of samples

   data = data';
   N=length(data);
   dt=1/N;

   % Compute the matrices of trigonometric functions

   p=1:N/2+1;
   n=1:N;
   tn=n*dt;

   % Computer the sine and cosine values

   C=cos(2*pi*n'*(p-1)/N);
   S=sin(2*pi*n'*(p-1)/N);

   % Compute Fourier Coefficients

   A=2/N*data*C;
   B=2/N*data*S;

   A(N/2+1)=A(N/2+1)/2;
```

```
% Return Coefficients

figure(1);
hold on;
ynew=C(:,order+1)*A(order+1)'+S(:,order+1)*B(order+1)';
xnew=n/N*360;
plot(xnew,ynew,'b')

for counter=1:20
   ynew=C(:,counter)*A(counter)'+S(:,counter)*B(counter)';
   maximum=max(ynew);
   minimum=min(ynew);
   value=maximum-minimum;
   graphmatrix(counter,1)=counter-1;
   graphmatrix(counter,2)=value;
end

amplitudes=graphmatrix;
```

C. FREQUENCY RESPONSE OF PHILIPS CT SCANNER

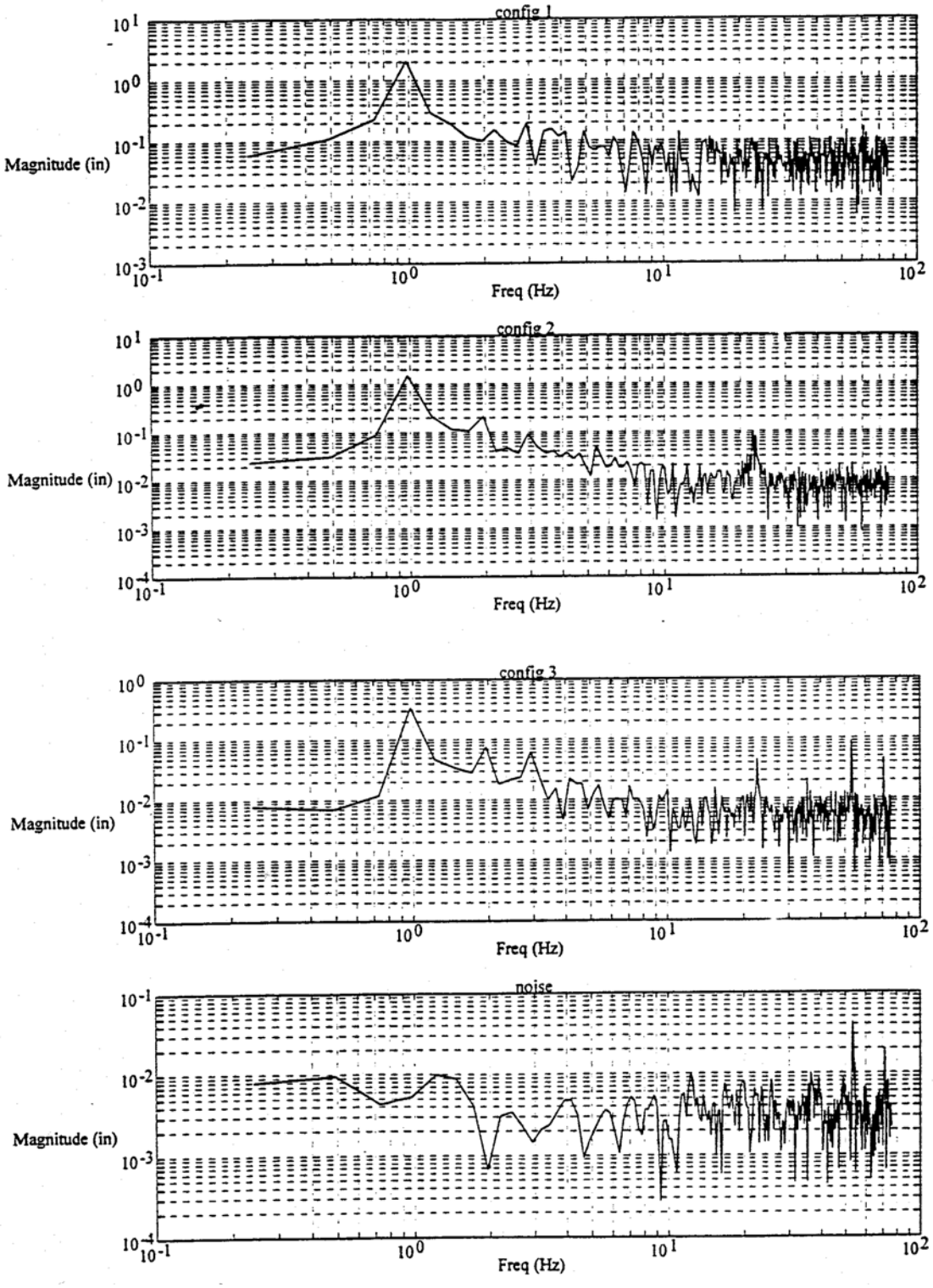

D. RK-4 TEST RIG SPECIFICATIONS

Basic Rotor Specifications:

Power:	95 to 125 Vac, Single Phase Or 190 to 250 Vac, single phase, 50 to 60 Hz at 3.0 A maximum.
Fuse Rating	250 V at 3 A slow-blow
Buffered Proximitor:	200 mV/mil
Max Speed:	10,000 rpm
Max Ramp Rate:	±15,000 rpm/min.

Mechanical Base Dimensions:

Height:	165 mm
Width:	340 mm
Depth:	789 mm

Motor Speed Control Dimensions:

Height:	115 mm
Width:	260 mm
Depth:	325 mm

Proximitor Assembly Dimensions:

Height:	86 mm
Width:	154 mm
Depth:	158 mm
Shaft Diameter	10 mm

E. FLEXBAL PROGRAM OUTPUT

```
 PROBES   SPEEDS   PLANES
  2        1        2

 PROBE CALIBRATION FACTORS

 PROBE    READING BY
  1        1.000
  2        1.000

 UNCORRECTED ROTOR

                    WITH RUNOUT                MINUS RUNOUT
 PROBE   SPEED   AMPLITUDE   PHASE, DEG.    AMPLITUDE   PHASE, DEG.
  1     1912.0   4.050         82.0          4.050         82.0
  2     1912.0   4.500        353.0          4.500        353.0

 TRIAL WEIGHT IN BALANCE PLANE 1

 TRIAL WEIGHT = 0.2000       ANGLE =   0.0 DEG

                WITH RUNOUT          MINUS RUNOUT     INFLUENCE COEFFICIENT
 PROBE  SPEED  AMPLITUDE  PHASE  AMPLITUDE  PHASE  AMPLITUDE  PHASE
  1    1912.0  7.310     228.0   7.310     228.0   54.53     240.0
  2    1912.0  12.70     134.0   12.70     134.0   82.21     143.9

 TRIAL WEIGHT IN BALANCE PLANE 2

 TRIAL WEIGHT = 0.2000       ANGLE =   0.0 DEG

                WITH RUNOUT          MINUS RUNOUT     INFLUENCE COEFFICIENT
 PROBE  SPEED  AMPLITUDE  PHASE  AMPLITUDE  PHASE  AMPLITUDE  PHASE
  1    1912.0  7.590     225.0   7.590     225.0   55.48     237.7
  2    1912.0  13.50     145.0   13.50     145.0   88.00     151.9

 NEW INFLUENCE COEFFICIENTS STORED IN INFRK4

 CORRECTION WEIGHTS

 PLANE     WEIGHT      ANGLE, DEG.   X COMPONENT Y COMPONENT
  1       0.1241        39.7         0.9553E-01  0.7922E-01
  2       0.1084       253.7        -0.3041E-01 -0.1041
```